

TABLE 1  
MAJOR STELLAR LIFETIMES (MYR)

| $M(M_{\odot})$ | PMS  | H   | He   |
|----------------|------|-----|------|
| 4.0            | 1.63 | 104 | 10.9 |
| 5.0            | 1.11 | 62  | 9.8  |
| 6.0            | 0.77 | 43  | 6.3  |
| 7.0            | 0.52 | 32  | 4.1  |
| 8.0            | 0.51 | 25  | 2.8  |

From column 1 to 4: stellar mass, pre main sequence lifetime, central H-burning phase lifetime, central He-burning phase lifetime

TABLE 2  
PROPERTIES OF THE MODELS AT THE END OF THE E-AGB

| M ( $M_{\odot}$ ) | $\beta$ | $M_H(M_{\odot})$ | ${}^4\text{He}$ | ${}^{12}\text{C}$     | ${}^{14}\text{N}$     | ${}^{16}\text{O}$     |
|-------------------|---------|------------------|-----------------|-----------------------|-----------------------|-----------------------|
| 4.0               | 0       | 0.8012           | 0.358           | $1.01 \cdot 10^{-14}$ | $1.04 \cdot 10^{-12}$ | $2.32 \cdot 10^{-14}$ |
| 5.0               | 0       | 0.8861           | 0.365           | $9.47 \cdot 10^{-10}$ | $4.29 \cdot 10^{-10}$ | $4.99 \cdot 10^{-11}$ |
| 6.0               | 0       | 0.9330           | 0.367           | $8.44 \cdot 10^{-8}$  | $8.29 \cdot 10^{-10}$ | $1.17 \cdot 10^{-10}$ |
| 7.0               | 0       | 0.9875           | 0.369           | $2.08 \cdot 10^{-6}$  | $1.59 \cdot 10^{-9}$  | $2.88 \cdot 10^{-9}$  |
| 7.0               | 0.005   | 0.9871           | 0.369           | $2.12 \cdot 10^{-6}$  | $1.59 \cdot 10^{-9}$  | $2.96 \cdot 10^{-9}$  |
| 7.0               | 0.01    | 0.9870           | 0.370           | $2.13 \cdot 10^{-6}$  | $1.59 \cdot 10^{-9}$  | $2.99 \cdot 10^{-9}$  |
| 7.0               | 0.02    | 0.9867           | 0.370           | $2.16 \cdot 10^{-6}$  | $1.59 \cdot 10^{-9}$  | $3.04 \cdot 10^{-9}$  |

From column 1 to 7: the stellar mass, the assumed value of  $\beta$  (see section 2), the mass of the He core and the surface mass fraction of  ${}^4\text{He}$ ,  ${}^{12}\text{C}$ ,  ${}^{14}\text{N}$  and  ${}^{16}\text{O}$ .

TABLE 3  
 SELECTED PROPERTIES OF THE 7  $M_{\odot}$  TP-AGB MODELS ( $\beta = 0.005$ )

| $M_H (M_{\odot})$ | $\Delta t_{ip} (10^3 \text{ yr})$ | $\log L_{He}^{max} (L_{\odot})$ | $\log T_H$ | $\log \rho_{He}$ | $^{12}\text{C}$       | $^{14}\text{N}$       | $^{16}\text{O}$       |
|-------------------|-----------------------------------|---------------------------------|------------|------------------|-----------------------|-----------------------|-----------------------|
| 0.9895            |                                   | 4.84                            | 8.070      | 3.530            | $2.229 \cdot 10^{-6}$ | $1.598 \cdot 10^{-9}$ | $3.173 \cdot 10^{-9}$ |
| 0.9899            | 1.60                              | 5.02                            | 8.076      | 3.563            | $2.229 \cdot 10^{-6}$ | $1.598 \cdot 10^{-9}$ | $3.173 \cdot 10^{-9}$ |
| 0.9903            | 1.62                              | 5.14                            | 8.079      | 3.612            | $2.229 \cdot 10^{-6}$ | $1.602 \cdot 10^{-9}$ | $3.173 \cdot 10^{-9}$ |
| 0.9908            | 1.63                              | 5.25                            | 8.085      | 3.616            | $2.229 \cdot 10^{-6}$ | $1.675 \cdot 10^{-9}$ | $3.174 \cdot 10^{-9}$ |
| 0.9913            | 1.64                              | 5.34                            | 8.089      | 3.647            | $2.229 \cdot 10^{-6}$ | $1.771 \cdot 10^{-9}$ | $3.174 \cdot 10^{-9}$ |
| 0.9917            | 1.65                              | 5.43                            | 8.092      | 3.672            | $2.229 \cdot 10^{-6}$ | $1.887 \cdot 10^{-9}$ | $3.175 \cdot 10^{-9}$ |
| 0.9922            | 1.65                              | 5.50                            | 8.096      | 3.687            | $2.228 \cdot 10^{-6}$ | $2.043 \cdot 10^{-9}$ | $3.175 \cdot 10^{-9}$ |
| 0.9927            | 1.64                              | 5.56                            | 8.098      | 3.715            | $2.228 \cdot 10^{-6}$ | $2.224 \cdot 10^{-9}$ | $3.176 \cdot 10^{-9}$ |
| 0.9931            | 1.63                              | 5.62                            | 8.101      | 3.715            | $2.228 \cdot 10^{-6}$ | $2.424 \cdot 10^{-9}$ | $3.177 \cdot 10^{-9}$ |
| 0.9936            | 1.63                              | 5.67                            | 8.102      | 3.740            | $2.228 \cdot 10^{-6}$ | $2.642 \cdot 10^{-9}$ | $3.177 \cdot 10^{-9}$ |
| 0.9940            | 1.62                              | 5.72                            | 8.105      | 3.755            | $2.228 \cdot 10^{-6}$ | $2.884 \cdot 10^{-9}$ | $3.178 \cdot 10^{-9}$ |
| 0.9945            | 1.61                              | 5.76                            | 8.106      | 3.764            | $2.227 \cdot 10^{-6}$ | $3.141 \cdot 10^{-9}$ | $3.179 \cdot 10^{-9}$ |
| 0.9949            | 1.60                              | 5.79                            | 8.109      | 3.781            | $2.227 \cdot 10^{-6}$ | $3.414 \cdot 10^{-9}$ | $3.180 \cdot 10^{-9}$ |
| 0.9953            | 1.89                              | 6.29                            | 8.074      | 3.885            | $4.156 \cdot 10^{-6}$ | $8.911 \cdot 10^{-6}$ | $2.801 \cdot 10^{-7}$ |
| 0.9957            | 1.84                              | 6.43                            | 8.059      | 3.918            | $1.044 \cdot 10^{-5}$ | $1.643 \cdot 10^{-5}$ | $6.786 \cdot 10^{-7}$ |
| 0.9960            | 1.92                              | 6.58                            | 8.050      | 3.928            | $1.966 \cdot 10^{-5}$ | $2.534 \cdot 10^{-5}$ | $1.254 \cdot 10^{-6}$ |
| 0.9964            | 1.93                              | 6.67                            | 8.044      | 3.953            | $3.150 \cdot 10^{-5}$ | $3.424 \cdot 10^{-5}$ | $1.958 \cdot 10^{-6}$ |
| 0.9967            | 1.94                              | 6.76                            | 8.040      | 3.973            | $4.524 \cdot 10^{-5}$ | $4.328 \cdot 10^{-5}$ | $2.757 \cdot 10^{-6}$ |
| 0.9970            | 1.93                              | 6.83                            | 8.036      | 3.989            | $6.040 \cdot 10^{-5}$ | $5.222 \cdot 10^{-5}$ | $3.625 \cdot 10^{-6}$ |
| 0.9974            | 1.93                              | 6.88                            | 8.034      | 4.004            | $7.672 \cdot 10^{-5}$ | $6.134 \cdot 10^{-5}$ | $4.560 \cdot 10^{-6}$ |

From column 1 to 8: position of the H-burning shell at the onset of the thermal pulse, duration of the inter-pulse, peak luminosity of the He-flash, temperature of the H-burning shell at He re-ignition, density of the He-burning shell at He re-ignition, surface mass fraction of  $^{12}\text{C}$ ,  $^{14}\text{N}$  and  $^{16}\text{O}$ .

TABLE 4  
 SELECTED PROPERTIES OF THE 7  $M_{\odot}$  TP-AGB MODELS ( $\beta = 0.01$ )

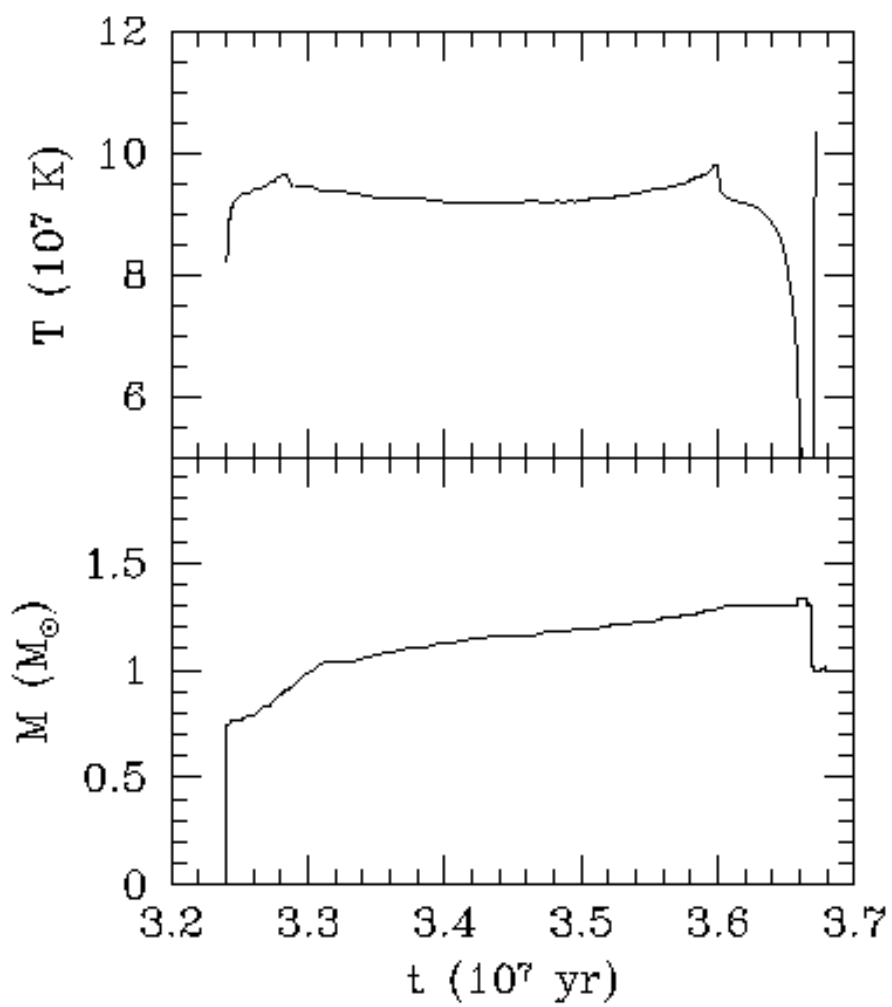
| $M_H (M_{\odot})$ | $\Delta t_{ip} (10^3 \text{ yr})$ | $\log L_{He}^{max} (L_{\odot})$ | $\log T_H$ | $\log \rho_{He}$ | $^{12}\text{C}$       | $^{14}\text{N}$       | $^{16}\text{O}$       |
|-------------------|-----------------------------------|---------------------------------|------------|------------------|-----------------------|-----------------------|-----------------------|
| 0.9897            |                                   | 5.04                            | 8.076      | 3.572            | $2.229 \cdot 10^{-6}$ | $1.598 \cdot 10^{-9}$ | $3.173 \cdot 10^{-9}$ |
| 0.9901            | 1.69                              | 5.17                            | 8.081      | 3.613            | $2.229 \cdot 10^{-6}$ | $1.602 \cdot 10^{-9}$ | $3.173 \cdot 10^{-9}$ |
| 0.9906            | 1.71                              | 5.28                            | 8.086      | 3.628            | $2.229 \cdot 10^{-6}$ | $1.674 \cdot 10^{-9}$ | $3.174 \cdot 10^{-9}$ |
| 0.9911            | 1.73                              | 5.38                            | 8.090      | 3.662            | $2.229 \cdot 10^{-6}$ | $1.773 \cdot 10^{-9}$ | $3.174 \cdot 10^{-9}$ |
| 0.9916            | 1.75                              | 5.46                            | 8.092      | 3.692            | $2.229 \cdot 10^{-6}$ | $1.896 \cdot 10^{-9}$ | $3.175 \cdot 10^{-9}$ |
| 0.9920            | 1.74                              | 5.54                            | 8.095      | 3.693            | $2.228 \cdot 10^{-6}$ | $2.056 \cdot 10^{-9}$ | $3.175 \cdot 10^{-9}$ |
| 0.9925            | 1.74                              | 5.60                            | 8.098      | 3.716            | $2.228 \cdot 10^{-6}$ | $2.250 \cdot 10^{-9}$ | $3.176 \cdot 10^{-9}$ |
| 0.9930            | 1.73                              | 5.66                            | 8.102      | 3.745            | $2.228 \cdot 10^{-6}$ | $2.461 \cdot 10^{-9}$ | $3.177 \cdot 10^{-9}$ |
| 0.9934            | 1.73                              | 5.71                            | 8.104      | 3.753            | $2.228 \cdot 10^{-6}$ | $2.689 \cdot 10^{-9}$ | $3.177 \cdot 10^{-9}$ |
| 0.9939            | 1.73                              | 5.76                            | 8.105      | 3.774            | $2.228 \cdot 10^{-6}$ | $2.947 \cdot 10^{-9}$ | $3.178 \cdot 10^{-9}$ |
| 0.9943            | 1.72                              | 5.81                            | 8.107      | 3.778            | $2.227 \cdot 10^{-6}$ | $3.222 \cdot 10^{-9}$ | $3.179 \cdot 10^{-9}$ |
| 0.9944            | 3.15                              | 6.73                            | 8.037      | 3.934            | $1.370 \cdot 10^{-5}$ | $6.670 \cdot 10^{-5}$ | $5.947 \cdot 10^{-6}$ |
| 0.9947            | 2.92                              | 6.81                            | 8.035      | 3.968            | $2.495 \cdot 10^{-5}$ | $9.167 \cdot 10^{-5}$ | $6.502 \cdot 10^{-6}$ |
| 0.9948            | 2.98                              | 6.99                            | 8.032      | 3.995            | $3.971 \cdot 10^{-5}$ | $1.259 \cdot 10^{-4}$ | $7.671 \cdot 10^{-6}$ |
| 0.9951            | 2.84                              | 7.02                            | 8.029      | 4.008            | $5.542 \cdot 10^{-5}$ | $1.525 \cdot 10^{-4}$ | $8.448 \cdot 10^{-6}$ |
| 0.9951            | 2.78                              | 7.17                            | 8.025      | 4.041            | $7.347 \cdot 10^{-5}$ | $1.949 \cdot 10^{-4}$ | $1.081 \cdot 10^{-5}$ |
| 0.9954            | 2.48                              | 7.20                            | 8.026      | 4.019            | $8.965 \cdot 10^{-5}$ | $2.145 \cdot 10^{-4}$ | $1.143 \cdot 10^{-5}$ |
| 0.9956            | 2.47                              | 7.22                            | 8.025      | 4.022            | $1.109 \cdot 10^{-4}$ | $2.361 \cdot 10^{-4}$ | $1.247 \cdot 10^{-5}$ |

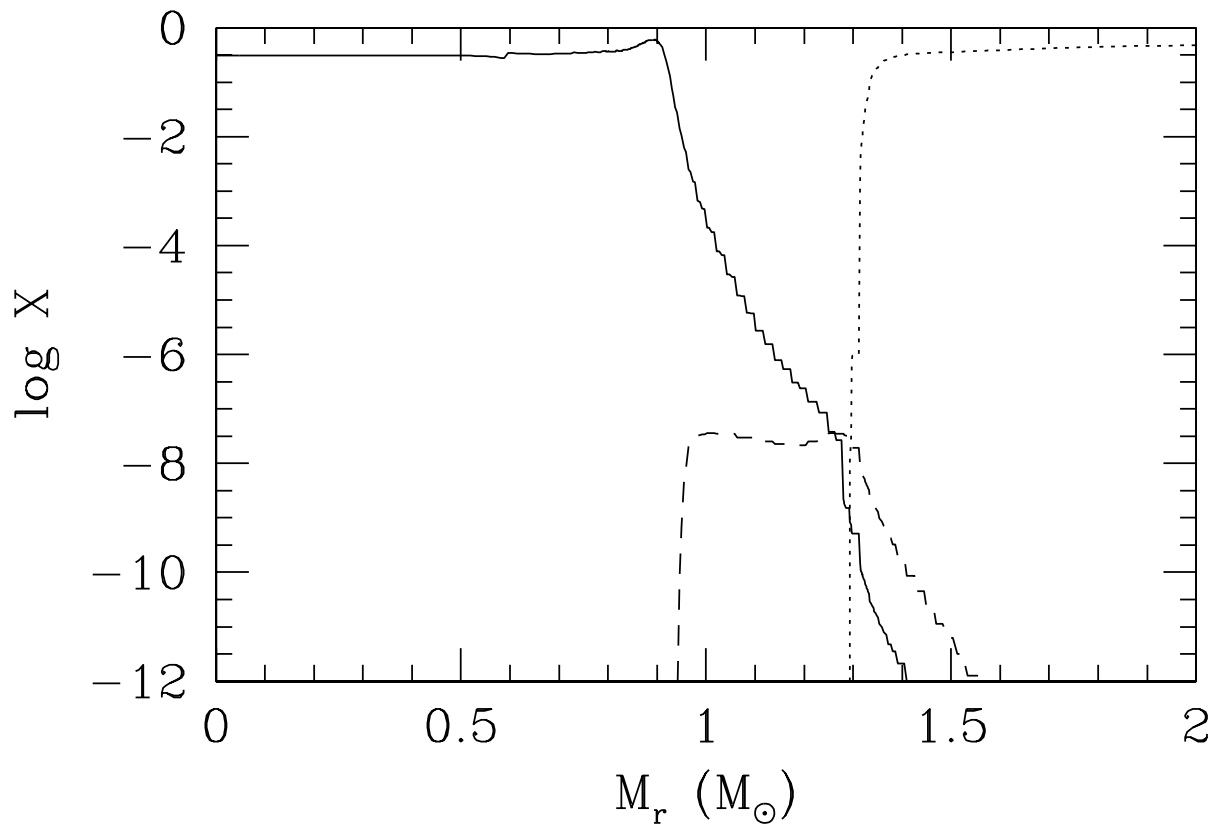
From column 1 to 8: position of the H-burning shell at the onset of the thermal pulse, duration of the inter-pulse, peak luminosity of the He-flash, temperature of the H-burning shell at He re-ignition, density of the He-burning shell at He re-ignition, surface mass fraction of  $^{12}\text{C}$ ,  $^{14}\text{N}$  and  $^{16}\text{O}$ .

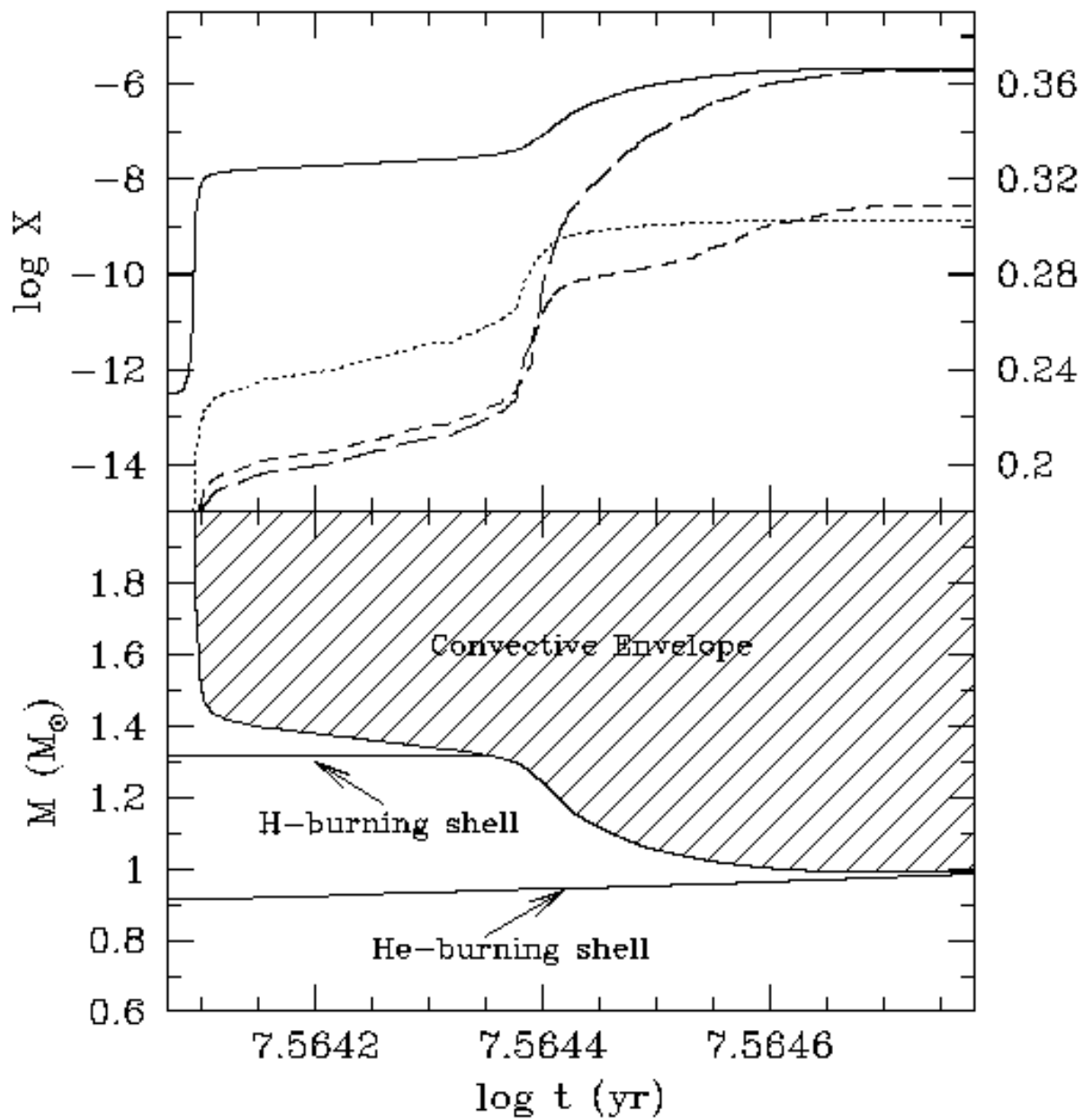
TABLE 5  
 SELECTED PROPERTIES OF THE 4  $M_{\odot}$  TP-AGB MODELS ( $\beta = 0.01$ )

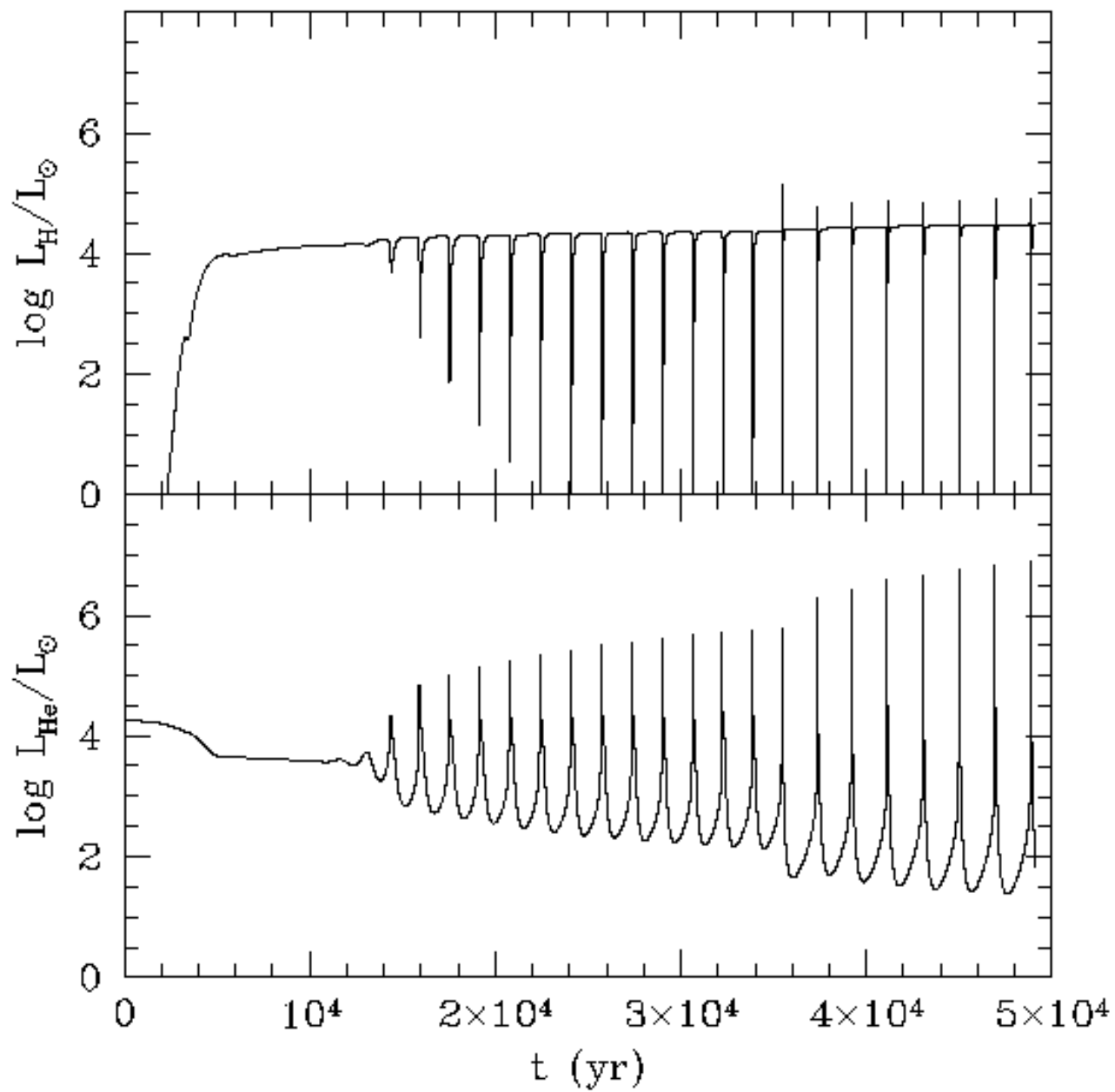
| $M_H (M_{\odot})$ | $\Delta t_{ip} (10^3 \text{ yr})$ | $\log L_{He}^{max} (L_{\odot})$ | $\log T_H$ | $\log \rho_{He}$ | $^{12}\text{C}$        | $^{14}\text{N}$        | $^{16}\text{O}$        |
|-------------------|-----------------------------------|---------------------------------|------------|------------------|------------------------|------------------------|------------------------|
| 0.8337            | 7.73                              | 4.80                            | 8.104      | 3.637            | $1.008 \cdot 10^{-14}$ | $1.043 \cdot 10^{-12}$ | $2.316 \cdot 10^{-14}$ |
| 0.8347            | 7.65                              | 5.48                            | 8.056      | 3.744            | $1.008 \cdot 10^{-14}$ | $1.043 \cdot 10^{-12}$ | $2.316 \cdot 10^{-14}$ |
| 0.8352            | 4.98                              | 4.93                            | 8.114      | 3.668            | $2.838 \cdot 10^{-13}$ | $1.371 \cdot 10^{-11}$ | $1.587 \cdot 10^{-13}$ |
| 0.8365            | 7.29                              | 6.09                            | 8.097      | 3.890            | $2.838 \cdot 10^{-13}$ | $1.371 \cdot 10^{-11}$ | $1.587 \cdot 10^{-13}$ |
| 0.8379            | 8.78                              | 6.33                            | 8.000      | 3.909            | $3.790 \cdot 10^{-6}$  | $3.857 \cdot 10^{-6}$  | $1.861 \cdot 10^{-7}$  |
| 0.8397            | 9.18                              | 6.41                            | 8.005      | 3.939            | $3.790 \cdot 10^{-6}$  | $3.858 \cdot 10^{-6}$  | $1.861 \cdot 10^{-7}$  |
| 0.8415            | 9.01                              | 6.52                            | 8.009      | 3.963            | $3.789 \cdot 10^{-6}$  | $3.858 \cdot 10^{-6}$  | $1.861 \cdot 10^{-7}$  |
| 0.8432            | 8.80                              | 6.59                            | 8.015      | 3.979            | $3.788 \cdot 10^{-6}$  | $3.859 \cdot 10^{-6}$  | $1.861 \cdot 10^{-7}$  |
| 0.8450            | 8.58                              | 6.65                            | 8.016      | 3.994            | $3.788 \cdot 10^{-6}$  | $3.860 \cdot 10^{-6}$  | $1.861 \cdot 10^{-7}$  |
| 0.8467            | 8.36                              | 6.71                            | 8.021      | 4.004            | $3.787 \cdot 10^{-6}$  | $3.861 \cdot 10^{-6}$  | $1.861 \cdot 10^{-7}$  |
| 0.8484            | 8.15                              | 6.75                            | 8.023      | 4.011            | $3.787 \cdot 10^{-6}$  | $3.861 \cdot 10^{-6}$  | $1.861 \cdot 10^{-7}$  |
| 0.8498            | 9.00                              | 7.19                            | 7.977      | 4.127            | $8.252 \cdot 10^{-5}$  | $3.861 \cdot 10^{-6}$  | $4.242 \cdot 10^{-6}$  |
| 0.8508            | 9.09                              | 7.37                            | 7.965      | 4.166            | $1.976 \cdot 10^{-4}$  | $3.866 \cdot 10^{-6}$  | $1.341 \cdot 10^{-5}$  |
| 0.8518            | 9.10                              | 7.49                            | 7.957      | 4.194            | $3.257 \cdot 10^{-4}$  | $3.875 \cdot 10^{-6}$  | $2.449 \cdot 10^{-5}$  |
| 0.8527            | 9.08                              | 7.59                            | 7.952      | 4.216            | $4.625 \cdot 10^{-4}$  | $3.890 \cdot 10^{-6}$  | $3.688 \cdot 10^{-5}$  |
| 0.8536            | 9.05                              | 7.67                            | 7.949      | 4.235            | $6.068 \cdot 10^{-4}$  | $3.909 \cdot 10^{-6}$  | $5.041 \cdot 10^{-5}$  |
| 0.8545            | 9.00                              | 7.74                            | 7.947      | 4.251            | $7.567 \cdot 10^{-4}$  | $3.933 \cdot 10^{-6}$  | $6.473 \cdot 10^{-5}$  |
| 0.8554            | 8.95                              | 7.80                            | 7.943      | 4.266            | $9.113 \cdot 10^{-4}$  | $3.961 \cdot 10^{-6}$  | $7.976 \cdot 10^{-5}$  |
| 0.8562            | 8.90                              | 7.86                            | 7.944      | 4.278            | $1.070 \cdot 10^{-3}$  | $3.993 \cdot 10^{-6}$  | $9.537 \cdot 10^{-5}$  |
| 0.8570            | 8.86                              | 7.90                            | 7.942      | 4.290            | $1.233 \cdot 10^{-3}$  | $4.028 \cdot 10^{-6}$  | $1.117 \cdot 10^{-4}$  |
| 0.8578            | 8.79                              | 7.94                            | 7.941      | 4.299            | $1.399 \cdot 10^{-3}$  | $4.068 \cdot 10^{-6}$  | $1.284 \cdot 10^{-4}$  |
| 0.8586            | 8.73                              | 7.98                            | 7.939      | 4.306            | $1.567 \cdot 10^{-3}$  | $4.112 \cdot 10^{-6}$  | $1.455 \cdot 10^{-4}$  |
| 0.8594            | 8.65                              | 8.01                            | 7.938      | 4.314            | $1.737 \cdot 10^{-3}$  | $4.160 \cdot 10^{-6}$  | $1.631 \cdot 10^{-4}$  |
| 0.8602            | 8.58                              | 8.04                            | 7.938      | 4.322            | $1.909 \cdot 10^{-3}$  | $4.282 \cdot 10^{-6}$  | $1.811 \cdot 10^{-4}$  |
| 0.8610            | 8.49                              | 8.07                            | 7.936      | 4.326            | $2.081 \cdot 10^{-3}$  | $4.520 \cdot 10^{-6}$  | $1.993 \cdot 10^{-4}$  |
| 0.8617            | 8.40                              | 8.09                            | 7.937      | 4.333            | $2.254 \cdot 10^{-3}$  | $4.984 \cdot 10^{-6}$  | $2.179 \cdot 10^{-4}$  |
| 0.8625            | 8.31                              | 8.12                            | 7.935      | 4.337            | $2.427 \cdot 10^{-3}$  | $5.901 \cdot 10^{-6}$  | $2.368 \cdot 10^{-4}$  |
| 0.8632            | 8.23                              | 8.13                            | 7.936      | 4.342            | $2.600 \cdot 10^{-3}$  | $7.681 \cdot 10^{-6}$  | $2.563 \cdot 10^{-4}$  |
| 0.8639            | 8.12                              | 8.15                            | 7.934      | 4.344            | $2.771 \cdot 10^{-3}$  | $1.083 \cdot 10^{-5}$  | $2.758 \cdot 10^{-4}$  |
| 0.8647            | 8.04                              | 8.15                            | 7.934      | 4.349            | $2.940 \cdot 10^{-3}$  | $1.615 \cdot 10^{-5}$  | $2.958 \cdot 10^{-4}$  |

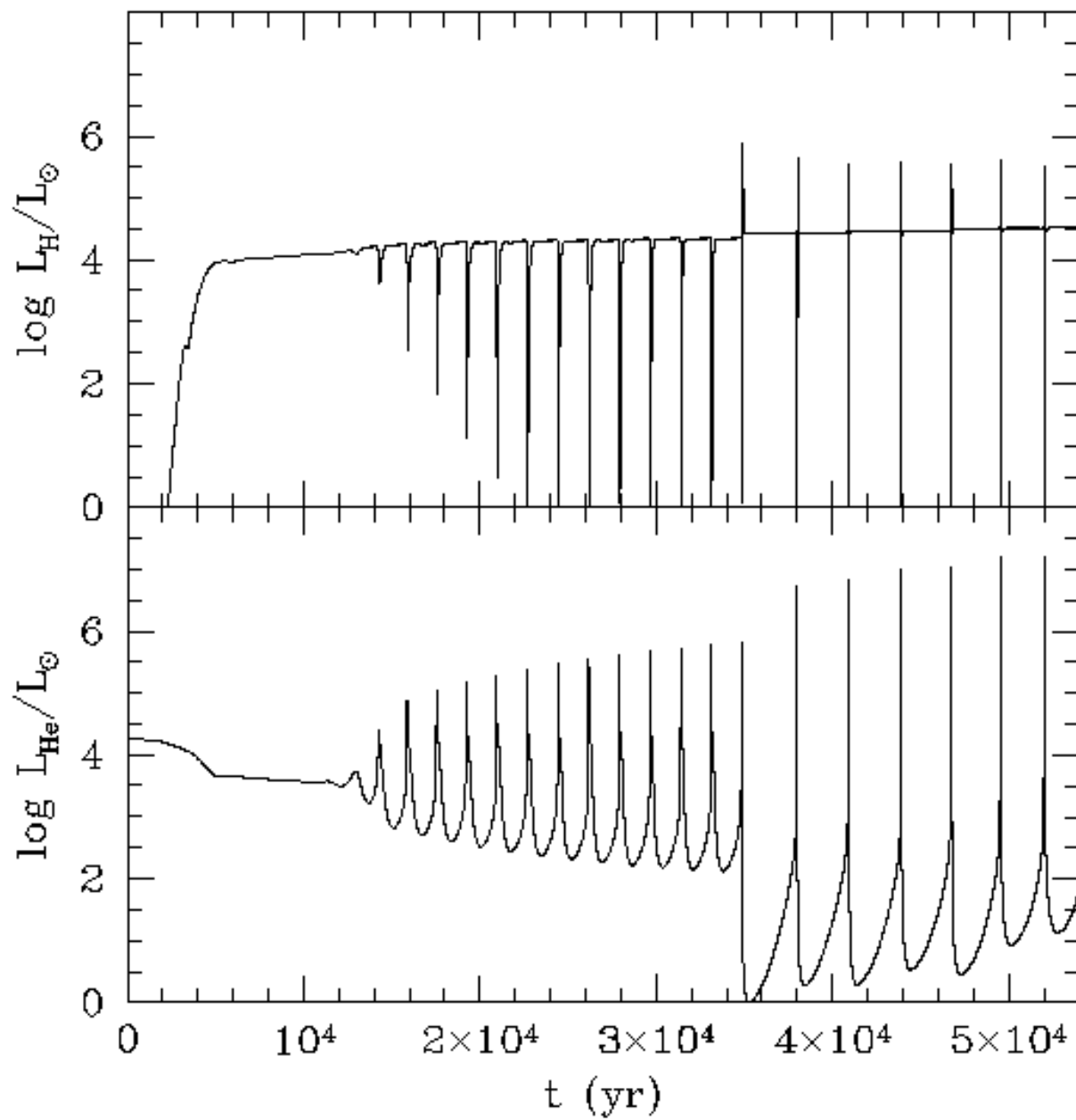
From column 1 to 8: position of the H-burning shell at the onset of the thermal pulse, duration of the inter-pulse, peak luminosity of the He-flash, temperature of the H-burning shell at He re-ignition, density of the He-burning shell at He re-ignition, surface mass fraction of  $^{12}\text{C}$ ,  $^{14}\text{N}$  and  $^{16}\text{O}$ .

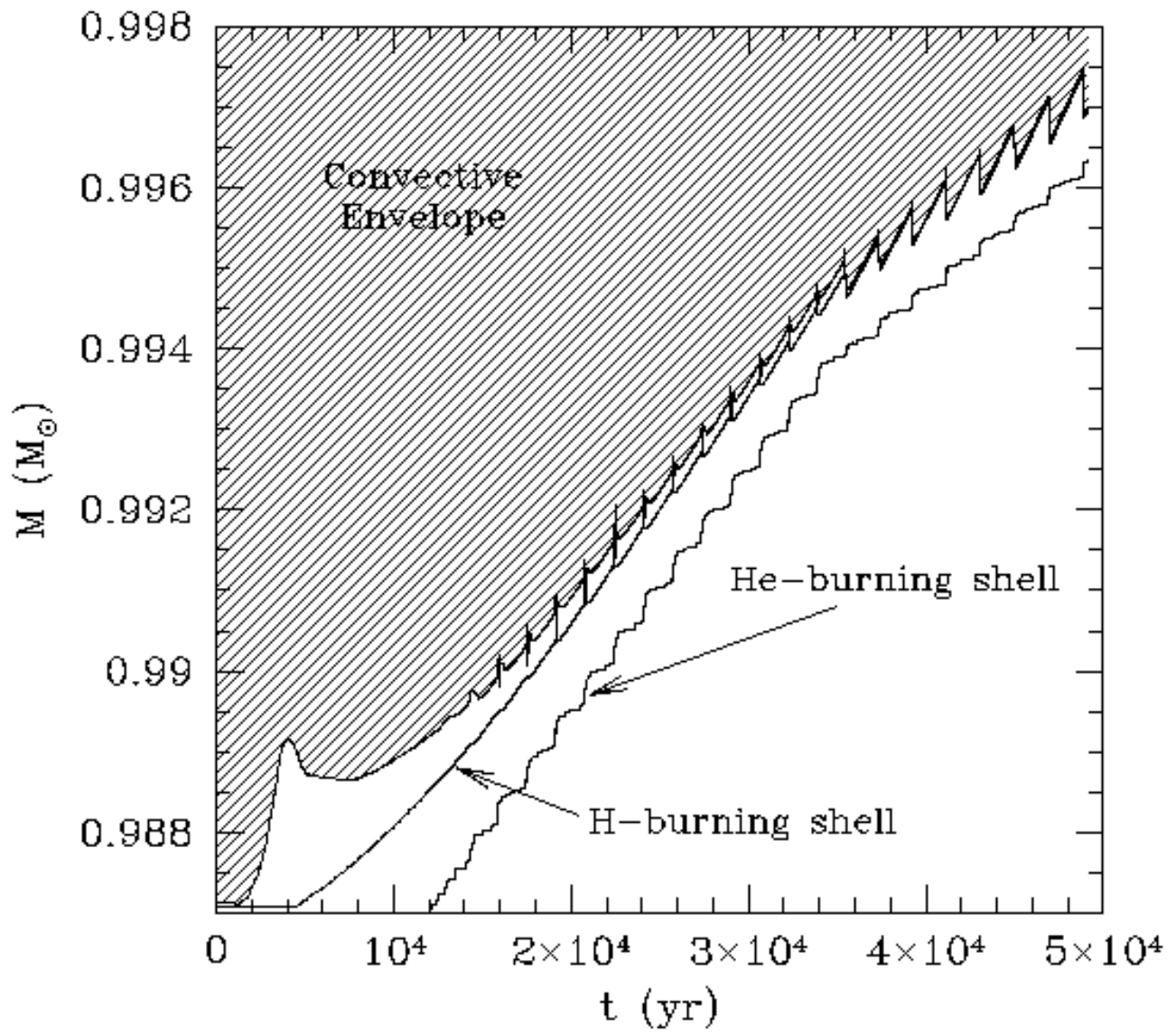


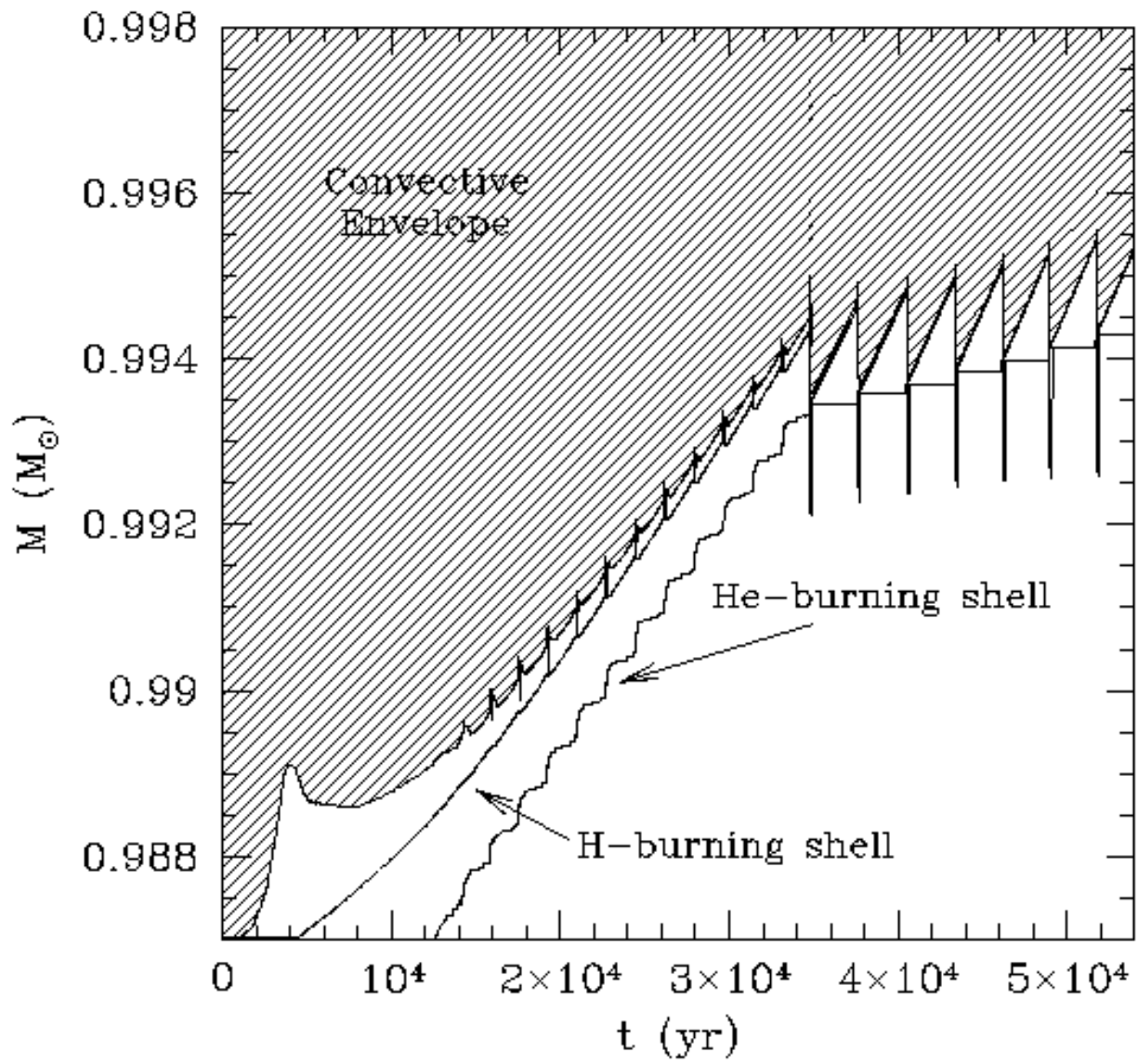


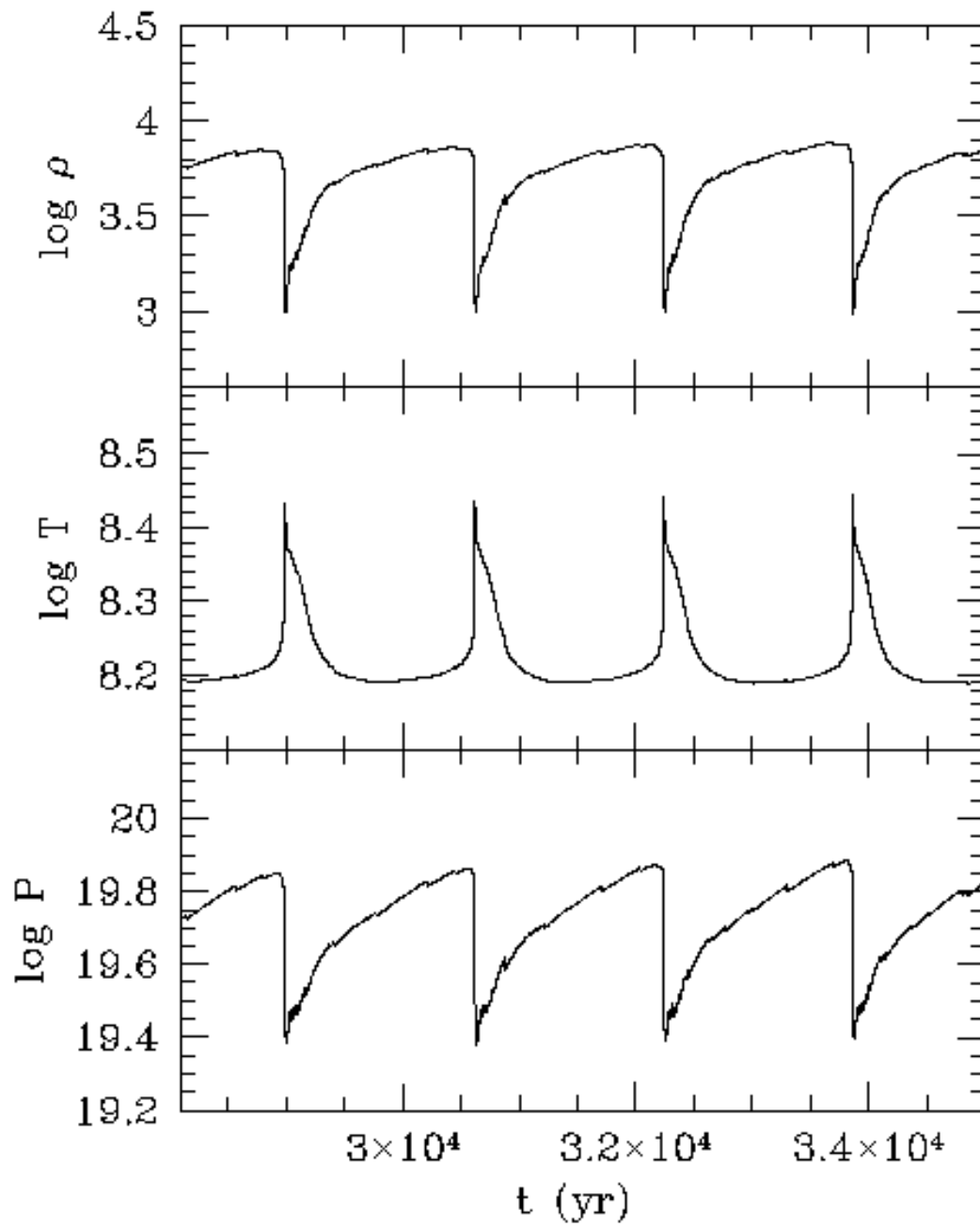


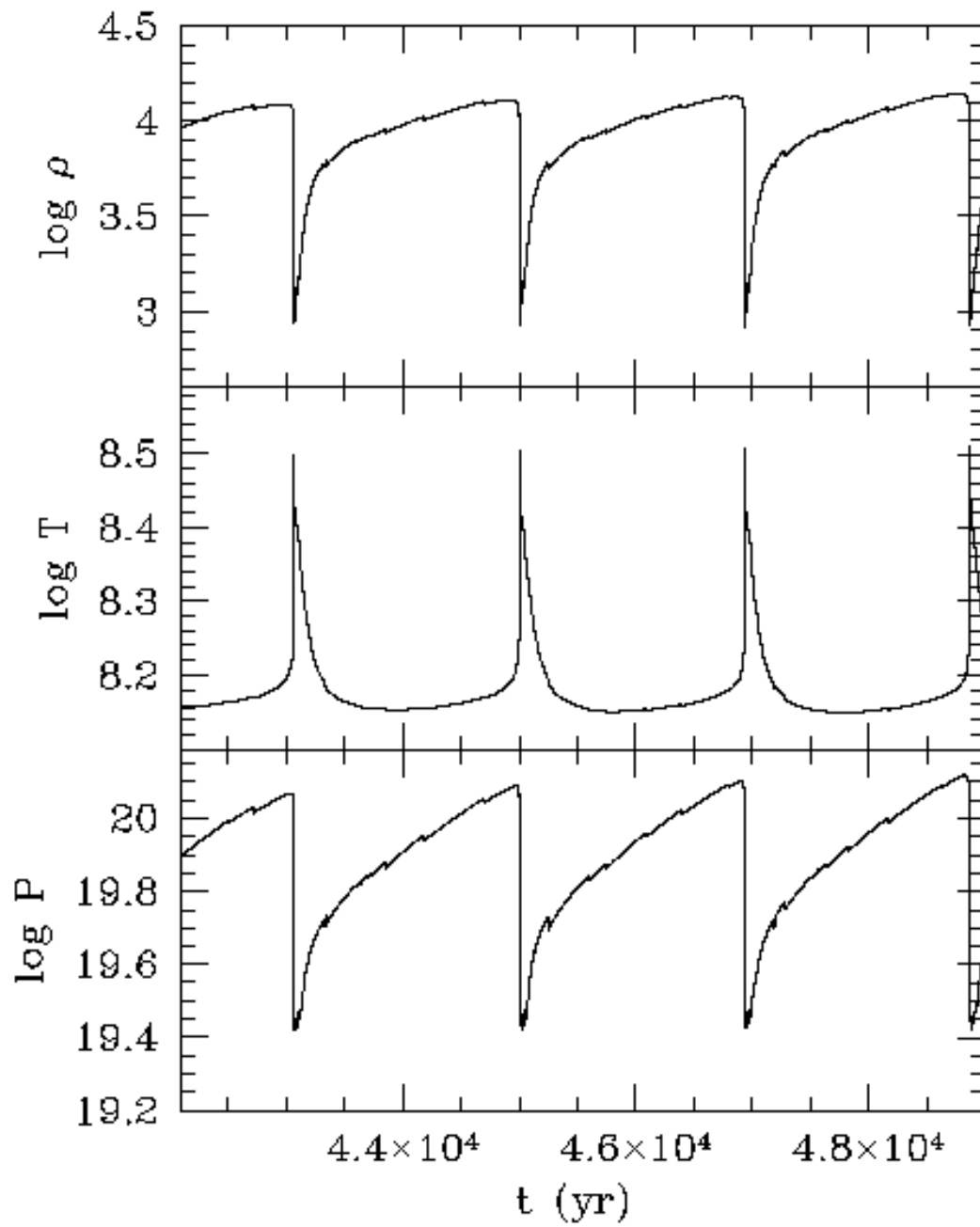


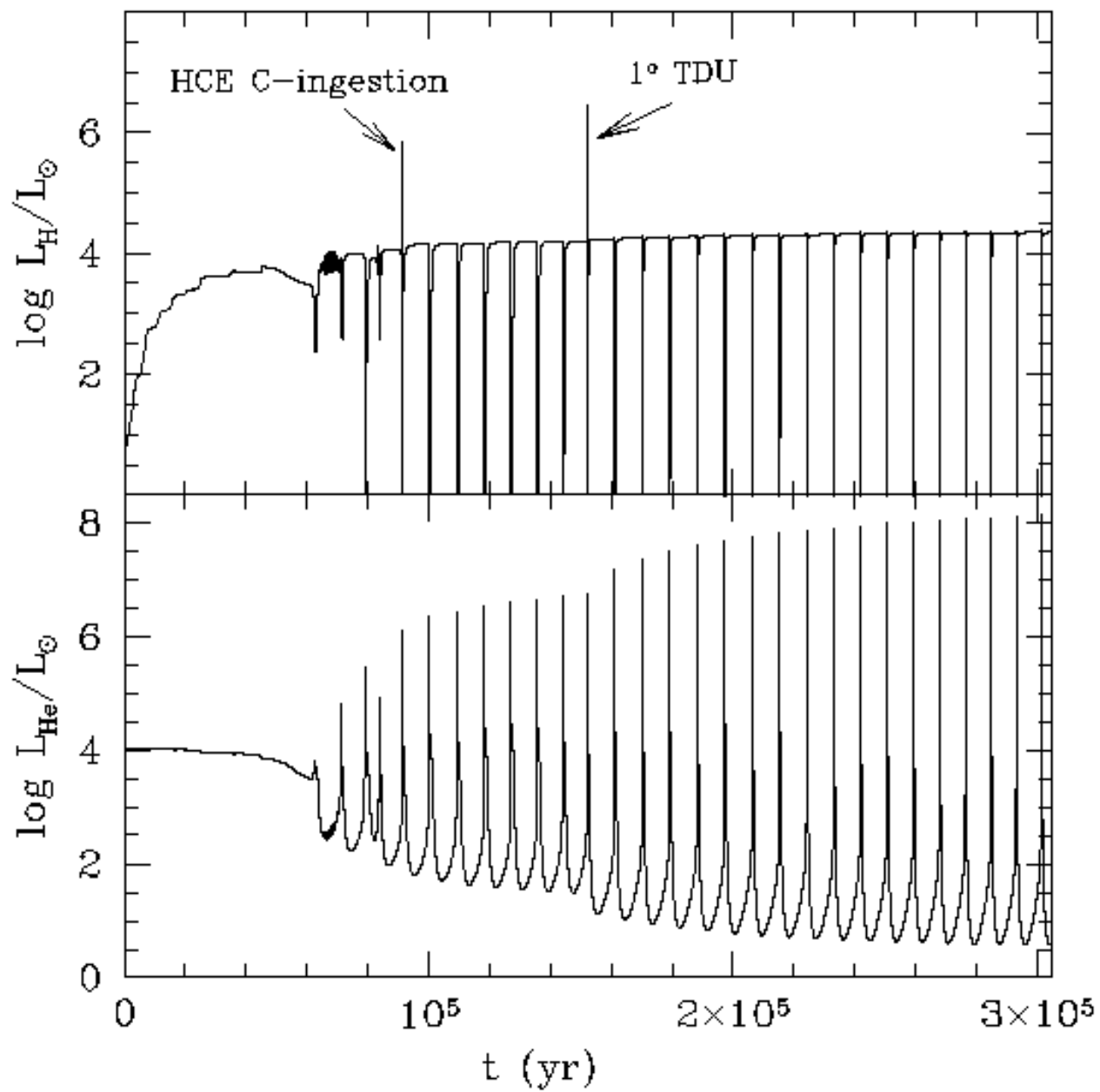


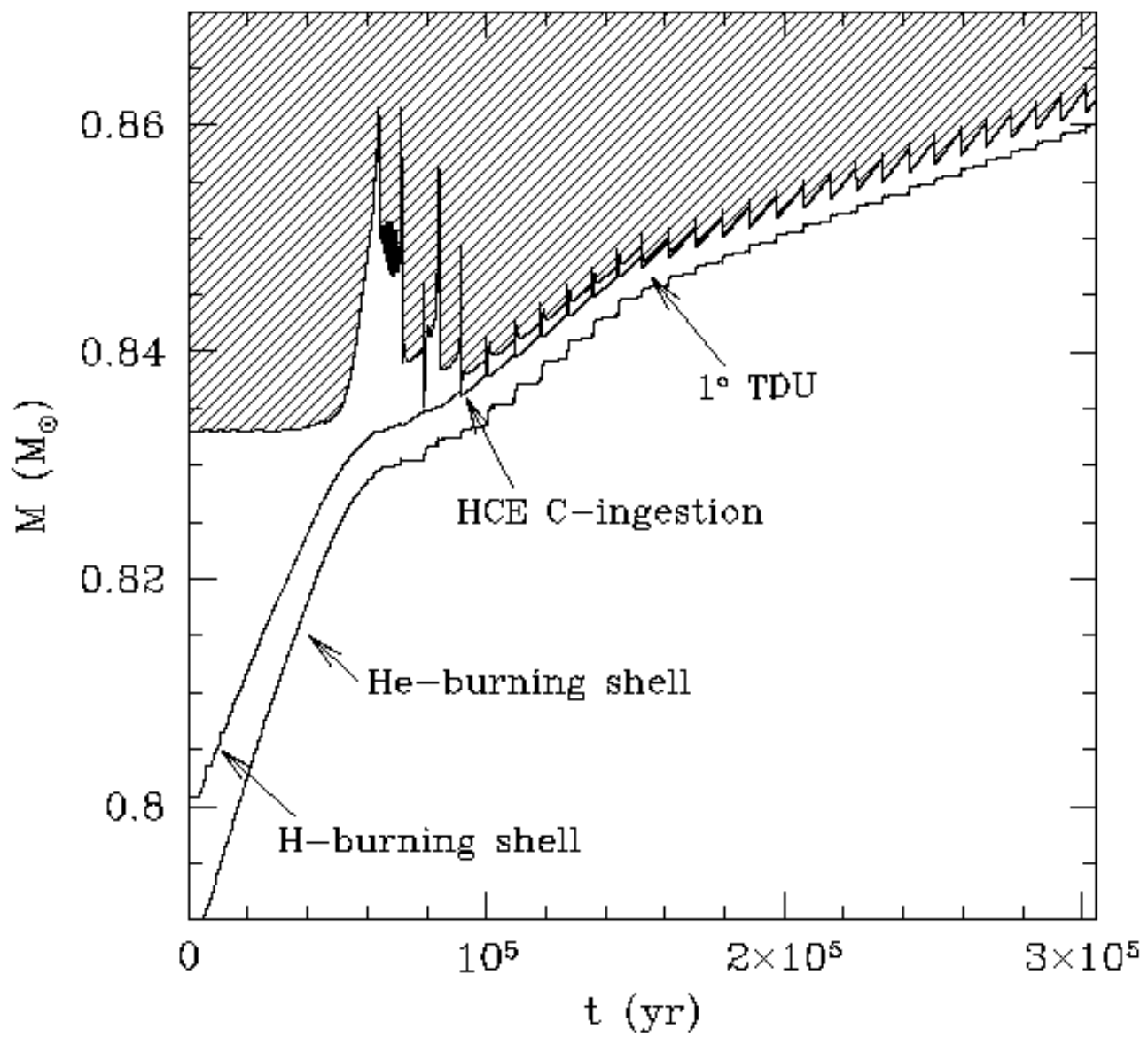


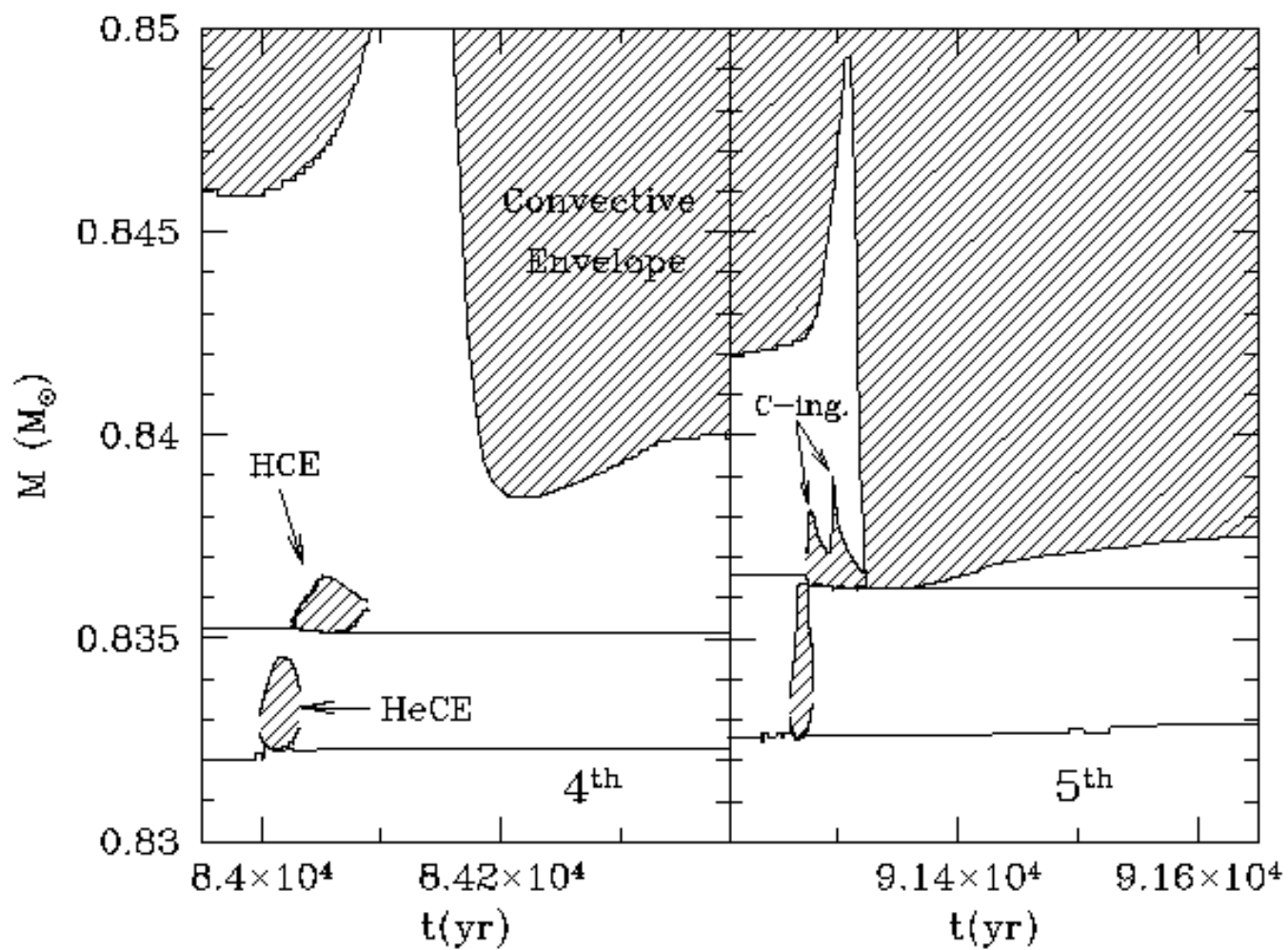












# EVOLUTION AND NUCLEOSYNTHESIS OF ZERO METAL INTERMEDIATE MASS STARS

Alessandro Chieffi

Istituto di Astrofisica Spaziale (CNR), via Fosso del Cavaliere, I-00133 Roma, Italy  
achieffi@ias.rm.cnr.it

Inma Domínguez

Dpto. de Física Teórica y del Cosmos, Universidad de Granada, 18071 Granada, Spain  
inma@ugr.es

Marco Limongi

Osservatorio Astronomico di Roma, Via Frascati 33, I-00040 Monteporzio Catone (Roma), Italy  
marco@nemo.mporzio.astro.it

and

Oscar Straniero

Osservatorio Astronomico di Collurania, I-64100 Teramo, Italy  
straniero@astrte.te.astro.it

Received \_\_\_\_\_; accepted \_\_\_\_\_

## ABSTRACT

New stellar models with mass ranging between 4 and 8  $M_{\odot}$ ,  $Z=0$  and  $Y=0.23$  are presented. The models have been evolved from the pre Main Sequence up to the Asymptotic Giant Branch (AGB). At variance with previous claims, we find that these updated stellar models *do* experience thermal pulses in the AGB phase. In particular we show that:

a) in models with mass larger than 6  $M_{\odot}$ , the second dredge up is able to raise the CNO abundance in the envelope enough to allow a *normal* AGB evolution, in the sense that the thermal pulses and the third dredge up settle on;

b) in models of lower mass, the efficiency of the CNO cycle in the H-burning shell is controlled by the carbon produced locally via the  $3\alpha$  reactions. Nevertheless the He-burning shell becomes thermally unstable after the early AGB. The expansion of the overlying layers induced by these weak He-shell flashes is not sufficient by itself to allow a deep penetration of the convective envelope. However, immediately after that, the maximum luminosity of the He flash is attained and a convective shell systematically forms at the base of the H-rich envelope. The innermost part of this convective shell probably overlaps the underlying C-rich region left by the inter-shell convection during the thermal pulse, so that fresh carbon is dredged up in a *hot* H-rich environment and a H flash occurs. This flash favours the expansion of the outermost layers already started by the weak thermal pulse and a deeper penetration of the convective envelope takes place. Then, the carbon abundance in the envelope rises to a level high enough that the further evolution of these models closely resembles that of more metal rich AGB stars.

These stars provide an important source of primary carbon and nitrogen, so a major revision of the chemical evolution in the early Galaxy is required. We suggest that the chemical imprint of these Pop III stars could be found in the old and metal poor components of the Milky Way.

## 1. Introduction

Evidence for an expanding Universe coupled to the observation of the fossil black body radiation leads to the natural conclusion that the primordial Universe was hot and dense and that there was an epoch during which nuclear reactions among neutrons and protons took place. A few hours after the Big Bang the primordial composition of the Universe was defined. The standard homogeneous Big Bang nucleosynthesis (as first computed by Fermi & Turkevich, for a recent analysis see Walker et al. 1991) predicts that the material which emerged from this epoch was mainly made up of  $^1\text{H}$ ,  $^4\text{He}$  and a small quantity of other light elements (D,  $^3\text{He}$  and  $^7\text{Li}$ ). The total mass fraction of heavier elements was lower than  $10^{-10}$ , so that the first generation of stars, the so called population III, was formed from a gas essentially lacking of metals. Such a peculiarity certainly influenced both the fragmentation of the primordial gas clouds and the evolutionary properties of this first stellar generation. In fact, in these extreme conditions, the cooling able to reduce the Jeans mass down to the stellar values was provided by the molecular hydrogen rather than by dust or heavy molecules and the progressive fragmentation was halted only when the gas became opaque due to the  $\text{H}_2$  line absorption (Carlberg 1981; Silk 1983; Lepp & Shull 1983; Palla, Salpeter & Stahler 1983; Yoshii & Saio 1986; Shapiro & Kang 1987; de Araújo & Opher 1989; Uehara, Susa & Nishi 1996; Haiman, Thoul & Loeb 1996; Omukai et al. 1998).

The initial mass function (IMF) emerging from this atypical star formation process has been the subject of a number of papers. Several groups have found that intermediate mass stars (IMS) could result from the fragmentation of primordial gas clouds. Yoshii and Saio (1986) found that the peak of the IMF for population III stars ranges between 4 and 8  $M_\odot$  while Uehara et al. (1996) derived that the minimum stellar mass is of the order of the Chandrasekhar mass (i.e.  $\sim 1.4 M_\odot$ ). Nakamura & Umemura (1999) concluded that the typical stellar mass is around  $3M_\odot$ ; this value may further increase by accretion of the environmental gas up to  $16 M_\odot$ . On the other hand, 3D simulations (Abel et al. 1997; Abel, Bryan & Norman 2000; Bromm, Coppi & Larson 1999) obtained a Jean mass of the order of  $10^2$ - $10^3 M_\odot$ ; their calculations, however, do not have enough resolution to explore further fragmentation into smaller masses. Recently, Nakamura & Umemura (2000) have performed 2D simulations and have found that the primordial IMF is likely to be bimodal, the first peak around  $2 M_\odot$  and the second peak between 10 and  $10^2 M_\odot$ , consistent with the previous cited works. Wasserburg & Qian (2000a, 2000b), by comparing iron and r-element abundances in very metal poor stars, have concluded that the first generation of galactic stars was essentially composed of massive objects ( $M \geq 100 M_\odot$ ) capable of producing a prompt iron synthesis. Following their model, the average galactic metallicity would increase up to  $[\text{Fe}/\text{H}] \sim -3$  in a few  $10^6$  yr. In

such a case even low mass stars could form after a very short time, but their iron content would be that of population II stars. So the actual IMF of population III stars is still an open question.

However, since the chemical composition of the matter ejected by a star largely depends on its mass, the study of the surface chemical composition of the most metal poor stars could help to shed light on the kind of stars which first populated our galaxy (and probably the Universe). Note, by the way, that the lifetime of the more massive IMS is short enough so that they could have really polluted the interstellar medium during the very early phase of dynamical collapse of our galaxy (masses larger than, say,  $\simeq 4 M_{\odot}$  live less than  $\simeq 10^8$  yr).

Great observational efforts have been made to identify very metal deficient stellar populations. The first attempt (Bond, 1981) failed to find stars with metallicity  $[\text{Fe}/\text{H}] < -3$ . Later on, a red giant with  $[\text{Fe}/\text{H}] \sim -4.5$  was identified by Bessel and Norris (1984) and since then the number of known low metallicity stars has increased somewhat (see e.g. Beers, Preston & Shectman 1992; Ryan, Norris & Bessel 1991) though only 6 of them have  $[\text{Fe}/\text{H}] \leq -3.5$ . Some authors suggest that 4 of these 6 stars have a metallicity  $[\text{Fe}/\text{H}] \sim -4$  (see Ryan, Norris & Beers 1996, 1999; Sneden et al. 1994; Primas et al. 1994; Ryan et al. 1991; Carney & Peterson 1991; Molaro & Castelli 1990; Molaro & Bonifacio 1990). To date, however, no stars having the primordial chemical composition (i.e.  $Z \sim 10^{-10}$  or  $[\text{Fe}/\text{H}] \sim -8.3$ ) have been found. Such a lack of "observable zero metal" stars actually supports the theoretical predictions that the primordial IMF did not favour the formation of low mass, long lived stars, but it does not rule out the primordial intermediate mass stars (P-IMS).

Though there is definite evidence that very metal poor stars (and also just metal poor stars) formed by matter strongly polluted at least by the ejecta of massive stars (consider, for example, the overabundance of the  $\alpha$  elements with respect to iron) there is some hint that a P-IMS generation formed: as an example, let us mention that the galactic nitrogen behaves as a primary element, i.e. it is solar scaled (although with an important dispersion around  $[\text{N}/\text{Fe}] \sim 0.0$ ) in the lower metallicity stars observed in the Milky Way (Laird 1985; Carbon et al. 1987). While the nucleosynthesis occurring in massive stars, exploding as type II supernovae, cannot account for this primary nitrogen component (see, for example, Timmes, Woosley & Weaver 1995), the presence of a generation of P-IMS could robustly contribute to the production of primary nitrogen.

It goes without saying that the inclusion or otherwise of the ejecta of a P-IMS generation in the general chemical evolution of a galaxy also alters drastically, the interpretation of the heavy element abundances

measured in the very low metallicity galactic stars and the intergalactic medium (IGM) at the high-redshifts (from  $z \sim 2$  to 4; Cowie et al. 1995; Tytler et al. 1995; Songaila & Cowie 1996; Pettini et al. 1997; Ellison et al. 2000).

For all these reasons we decided to revise the evolutionary properties and the related nucleosynthesis of these primordial stars in a wide range of stellar masses. In this way, we hope to identify the possible footprints left by the primordial stellar population in the galactic chemistry.

The necessity to calculate new P-IMS models derives from the fact that most of the available theoretical studies of this kind of stars stop at the end of the He-burning (Ezer 1961, 1972; Ezer & Cameron 1971; Eryurt-Ezer 1981; Castellani, Chieffi & Tornambè 1983; Tornambè & Chieffi 1986; Cassisi & Castellani 1993). As is well known, the most important contribution of the IMS to the galactic chemical evolution comes from the nucleosynthesis occurring during the thermally pulsing phase of the AGB. These stars, in fact, produce in their interior carbon, nitrogen and neutron rich isotopes which can enrich the interstellar medium by the combined efforts of the dredge up and the mass loss. In spite of their potential importance in nucleosynthesis and chemical evolution, to date just one paper has addressed the computation of AGB models of this generation of P-IMS (Chieffi & Tornambè 1984), the main finding (based on the evolution of a  $5 M_{\odot}$ ) being that these stars do not experience the thermally pulsing phase (see below). In a companion paper Fujimoto et al. (1984) addressed the general behaviour of the helium shell flashes in zero metal AGB stars by means of an analytical model: their conclusion was that the thermally pulsing phase takes place in stars less massive than  $4 M_{\odot}$ .

The scenario which emerged from those computations was that the overall impact of a P-IMS generation on the chemical evolution of the light elements (mainly C and N) in the galaxy was marginal. On the other hand, the lack of thermal pulses coupled to a reduced mass loss rate (due to the fact that these stars are significantly more compact and dimmer than the present ones) led the authors to suggest that these stars were more likely to increase the degenerate C-O core mass up to  $1.4 M_{\odot}$  and hence to explode as type I  $\frac{1}{2}$  supernovae. The result would be a strong pollution of the interstellar medium of material formed by elements produced by complete explosive Si burning (Fe, Co and Ni), incomplete explosive Si burning (Mn, Cr and V) and explosive O burning (Si, S, Ar, Ca and K).

In this paper and in a companion one (Limongi, Straniero & Chieffi 2001) we present a full set of evolutionary models of zero metal stars ranging in mass between 4 and  $25 M_{\odot}$ , from the pre main sequence up to the AGB or up to the iron core collapse. In particular this paper illustrates our results for models

having  $M \leq M_{up}$  (namely the smallest mass which ignites carbon off-centre in the degenerate core).

## 2. The models

The evolution of five P-IMS models, with mass 4, 5, 6, 7 and 8  $M_{\odot}$ ,  $Z=0$  and  $Y=0.23$ , has been computed starting from the pre-main sequence up to either an advanced phase on the AGB or up to the carbon ignition for the more massive model. These computations have been performed by means of the latest version of the FRANEC code, release 4.8 (see Chieffi, Limongi & Straniero 1998). Detailed references for the input physics adopted have been reported by Straniero, Chieffi & Limongi (1997). The main characteristic of this code is that the set of equations used to describe both the chemical evolution (due to the nuclear burning) and the physical structure are fully coupled and solved simultaneously. This coupling is required to follow the final phases of the evolution of massive stars, from the oxygen burning onwards. In order to produce a homogeneous set of models, we have adopted the same computational scheme for intermediate mass stars. The nuclear network used in the present computations includes 48 isotopes (269 reactions) for the H-burning, and 34 isotopes (147 reactions) for the He-burning (see Fig. 1). In order to identify the lowest stellar mass for which a degenerate carbon ignition occurs ( $M_{up}$ ), a reduced set of nuclear species and related reactions has been added for the carbon burning, namely 9 isotopes and 8 reactions. A revised version of the time dependent mixing scheme first introduced by Sparks & Endal (1980) has been adopted. In particular the mass fraction ( $X_j$ ) of a certain isotope at the mesh-point  $j$ , inside a convective region having total mass  $M_{conv}$ , is given by:

$$X_j = X_j^o + \frac{1}{M_{conv}} \sum_k (X_j^o - X_k^o) f_{j,k} \Delta M_k \quad (1)$$

where the summation is extended over the whole convective region and the superscript  $^o$  refers to unmixed abundances.  $\Delta M_k$  is the mass of the mesh-point  $k$ , while the damping factor  $f$  is:

$$f_{j,k} = \frac{\Delta t}{\tau_{j,k}} \quad (2)$$

if  $\Delta t < \tau_{j,k}$ , or

$$f_{j,k} = 1 \quad (3)$$

if  $\Delta t \geq \tau_{j,k}$ . Here  $\Delta t$  is the time step and  $\tau_{j,k}$  is the mixing turnover time between the mesh-points  $j$  and  $k$ , namely:

$$\tau_{j,k} = \int_{r(j)}^{r(k)} \frac{dr}{v(r)} = \sum_{i=j,k} \frac{\Delta r_i}{v_i} \quad (4)$$

The mixing velocity ( $v_i$ ) is computed according to the mixing length theory (Cox & Giuli 1968) and  $\Delta r_i$  is the length of the mesh-point  $i$ . This algorithm allows us to account for the partial mixing that occurs when the time step is reduced to or below the mixing timescale. This condition is sometimes fulfilled in the computation of advanced evolutionary phases. For example, thermally pulsing models require time steps of a few days (in some cases just a few hours) which may be comparable to or lower than the mixing timescale defined in equation (4). The borders of the convective regions are identified by means of the classical Schwarzschild criterion. Note that we have used, for the H-rich material, opacity tables computed by assuming  $Z = 10^{-4}$  and various ratios for the H and He abundances (Alexander & Ferguson, 1994; Iglesias, Rogers & Wilson 1992). These tables allow a suitable description of the radiation transport in the stellar envelope, as long as the metallicity does not exceed  $Z = 10^{-4}$ . For this reason, our evolutionary sequences become unreliable when the metallicity in the envelope, as modified by the third dredge up, increases over this value.

The computation of stellar models is usually based on semi-empirical (or phenomenological) descriptions of hydrodynamic phenomena occurring in real stars, namely convection and mass loss. The widely used *mixing length theory* of convection is a well known example of this phenomenological approach to stellar hydrodynamics. This procedure does not provide, in general, a satisfactory physical description of these complex phenomena. Nevertheless, once the stellar models are properly calibrated, it may allow us to obtain adequate predictions for the stellar properties. This may be done by *tuning* the models (i.e. by changing the parameters left free in the phenomenological theory) until they reproduce certain selected and well measured observable quantities. Unfortunately, due to the lack of an observational counterpart, such a procedure cannot be followed for  $Z=0$  models, so that the question of the calibration becomes particularly critical for population III stars. A possible alternative approach consists of adopting the values of the tuned free parameters obtained for larger metallicities. However, owing to the particular structure developed by metal deficient stars, an extrapolation of the calibrated parameters down to  $Z=0$  may induce a substantial error. Thus, in order to estimate the uncertainties implicit in the above description of the stellar hydrodynamics, one should explore a range of values for these free parameters that is as wide as possible, but this would imply the computation of a great number of stellar models. A general discussion of this very important problem is beyond the goals of the present paper. In the following we will focus our attention on those phenomena that particularly affect the estimated nucleosynthesis of the P-IMS stars.

Mass loss has a negligible effect on intermediate mass stars up to the onset of the AGB. Strong mass loss rates (between  $10^{-8}$  and  $10^{-4} M_{\odot}/\text{yr}$ ) are indeed observed in AGB stars. The duration of this phase,

the mass of the resulting compact stellar remnant and the chemical yields are then substantially affected by mass loss. Groenewegen & De Jong (1993, 1994a, 1994b), on the basis of synthetic AGB models, found that a Reimers (1975) mass loss rate with a multiplicative factor  $\eta \sim 4$  can reproduce the observed high-luminosity tail of the carbon stars luminosity function in our Galaxy and in the Magellanic Clouds as well as the observed abundances in LMC planetary nebulae. Domínguez et al. (1999) have shown that with such a mass loss rate the final masses of intermediate mass stellar models are compatible with the initial-final mass relation (Weidemann 1987; Herwig 1995). More recently other formulas have been proposed (Vassiliadis & Wood 1993; Blöcker 1995) that predict a huge mass loss rate for AGB stars (see, for a recent revision of the initial-to-final mass relation, Weidemann 2000). We do not know if a similar strong mass loss rate also characterizes population III AGB stars. It has been suggested (see, for example, Vassiliadis and Wood) that the increase of the mass loss rate during the AGB may be caused by the onset of large-amplitude radial pulsation. Whether P-IMS stars also suffered this kind of instability is a matter of opinion. The lower opacity of a metal deficient atmosphere generally implies more compact stars. This could reduce the mass loss rate. However, we find (see Section 4) that, as a consequence of the second and third dredge up, the P-IMS become C-rich. The carbon excess alters the structure of the atmosphere which might favour the formation of grains and increase the molecular blanketing, so that the opacity and, in turn, the mass loss rate could grow. Then, without an observational support, the actual mass loss rate that characterizes the AGB evolution of P-IMS is practically unknown. Note that the overall characteristics of the internal structure of an AGB star are generally dependent on two quantities: the core mass and the envelope mass (see, for example, Iben & Renzini 1983). However while the envelope mass is larger than  $1.5\text{--}2 M_{\odot}$  the main parameter is the core mass. Thus, since the initial envelope mass of an intermediate mass star is rather large, the internal structure remains weakly dependent on the mass loss for a large fraction of the AGB phase. The AGB stellar models presented here have been computed without mass loss. Our computations generally stopped before the onset of the mass loss-dominated AGB phase, even in the case of a particularly strong mass loss (except for the last computed thermal pulses of the lowest mass model).

An even more complex situation concerns stellar convection in AGB stars. It has been widely discussed whether the classical treatment of convection (both physical and numerical) is sufficient to describe the second and third dredge up occurring during the AGB phase, or whether they require an extra-mixing whose physical nature has still to be clarified, acting below the convective border (Iben 1975, 1981; Becker & Iben, 1979; Iben & Renzini 1982, 1983; Hollowel & Iben 1989; Lattanzio 1989; Castellani et al. 1990; Castellani,

Marconi & Straniero 1998; Herwig et al. 1997; Straniero et al 1997; Frost & Lattanzio 1996; Langer et al. 1999; Mowlavi 1999; Herwig 2000). In summary, when the inner border of the convective envelope approaches the H depleted (He enriched) region, even a small perturbation, perhaps driven by a moderate mechanical overshoot, may induce a substantial dredge up. In fact, as noted by Becker & Iben (1979; see also Castellani et al. 1990 and Frost & Lattanzio 1996), if the convective envelope (H-rich) penetrates a region that is progressively more He enriched, a discontinuity of the radiative gradient forms at the interface between the stable and unstable layers. This occurs because the H-rich envelope has a significantly greater opacity than the He-rich layer immediately below it. In such a case, if some mixing occurs below the inner border of the convective envelope, the local hydrogen abundance rises, the opacity (and the radiative gradient) grows and this layer becomes convectively unstable. A similar situation is encountered at the outer edge of the convective core during the central He-burning (Paczynsky 1970; Castellani, Giannone & Renzini 1971); in this case the discontinuity of the radiative gradient is caused by the conversion of helium (low opacity) into carbon and oxygen (high opacity) at the base of the convective core. Castellani et al. (1985) named this phenomenon *induced overshoot* (i.e. induced by the chemical discontinuity that forms at the boundary of a convective region) to be distinguished from the *mechanical overshoot* (i.e the mixing caused by the convective elements that conserve a finite velocity beyond the unstable region). Note that in the conditions discussed above, the existence of a small (in most cases negligible) mechanical overshoot may trigger a substantial induced overshoot. Castellani, Marconi & Straniero (1998) show that the overall impact on the second dredge up of this phenomenon is generally small. On the contrary, Frost & Lattanzio (1996, see also Herwig et al 1997; Herwig 2000 and Mowlavi 1999) found that the inclusion of a moderate overshoot strongly increases the efficiency of the third dredge up. Obviously a change in the strength of the third dredge up greatly affects the surface abundances of an AGB star. Thus, spectroscopic observation of the present-day AGB stars may be used to check the reliability of the various mixing algorithms and eventually to calibrate stellar models. Unfortunately the same cannot be done with the missing population III. Once again, due to the peculiarity of  $Z=0$  models, the descriptions obtained for more metal rich stars could be unreliable. The basic set of models presented here has been obtained by limiting the mixing within the borders defined by the Schwarzschild criterion. However we have computed some additional models to investigate the influence of a possible extra-mixing below the convective envelope on the AGB evolution of  $Z=0$  stars. Then, following to the hydrodynamic descriptions discussed by Herwig et al. (1997), we have tentatively assumed that the convective motions do not stop abruptly at the base of the convective unstable envelope, but decrease exponentially below it. More precisely, we have used the following expression for the

mixing velocity below the convective envelope:

$$v = v_{bce} \exp(-D/\beta H_p) \quad (5)$$

where  $v_{bce}$  is the mixing velocity at the base of the convective unstable envelope (as obtained by means of the mixing length theory),  $D$  is the distance from the stability border,  $H_p$  is the pressure scale height and  $\beta$  is a free parameter, which evidently determines the strength of the exponential decline. Herwig et al. (1997) suggest  $\beta = 0.02$  (actually they use  $f$  instead of  $\beta$ ) for solar metallicity models. We have used various values for  $\beta$  ranging between 0.005 and 0.04 (see Sections 4 and 5). Note that the extra-mixing provided by this formula is, in most cases, negligible. In fact, since in the framework of the mixing length theory the mixing velocity is proportional to the difference between the radiative and the adiabatic gradients, it falls to zero at the boundary of a convective region, where the condition of marginal stability (i.e.  $\nabla_{rad} = \nabla_{ad}$ ) is fulfilled. However, when the convective envelope moves inward, down to the region where the H has been converted into He, the discontinuity in the radiative gradient forms and  $v_{bce}$  grows. In such a case, the extra-mixing provided by equation (5) smooths out the chemical profile and prevents the formation of the discontinuity in the radiative gradient. In order to reduce possible numerical noises and save computational time, we do not apply equation (5) to the borders of other convective regions.

### 3. The central H and He-burning

The overall characteristics of the central H and He burning phases of our models do not substantially differ from the ones already found in previous studies of very metal poor stars (Ezer 1961, 1972; Ezer & Cameron 1971; Eryurt-Ezer 1981; Chieffi & Tornambè 1984; Tornambè & Chieffi 1986; Cassisi and Castellani 1993). A more quantitative comparison with the old models by Ezer and coworkers reveals major differences probably due to differences in the input physics. On the contrary, the models presented in the more recent papers are in good agreement with the present ones. This is no surprise because they were obtained by means of old versions of our code (the FRANEC). Small residual differences can easily be attributed to slightly different input physics.

In Table 1 we report the duration (in Myr) of the most relevant evolutionary phases, namely the pre-main sequence (PMS), the central H-burning and the central He-burning. Central temperatures versus central densities are plotted in Figure 2, while the HR diagrams are shown in Figure 3. The temporal evolutions of the central convective region up to the end of the central He-burning are illustrated, for each star, in Figure 4.

As has been clear since the pioneering papers, the approach to the MS and the central H-burning phase are influenced by the lack of CNO nuclei. In a more metal-rich IMS, in fact, the CNO cycle is the main energy supplier and since it has a very strong dependence on the temperature, the burning remains confined within the innermost part of the star and the convective core persists until the fuel is almost exhausted in the centre. In the case of these P-IMS, on the contrary, the nuclear energy might be produced only via the PP-chain (at least while the temperature remains below the threshold value for the activation of the  $3\alpha$  reactions) and since it has a weaker dependence on the temperature, the whole structure is necessarily much hotter and the active burning occurs in a more extended region around the centre. The lack of a burning strongly concentrated in the centre leads to the following characteristics: a) the convective core is much smaller than in more metal rich stars of similar mass and it even vanishes when the central mass fraction of H is still 0.5, and b) in almost 80% of the total mass of the star the He abundance increases. The lack of an extended convective core clearly influences the stellar track in the  $T_C - \rho_C$  plane (see Fig. 2): in particular, since the PP-chain never slows the gravitational contraction effectively, the central temperature and density continue to rise systematically until the  $3\alpha$  reactions start up. The abundance of carbon produced in the centre as a function of time is shown in Figure 5. When the  $^{12}\text{C}$  mass fraction is about  $10^{-10}$  the H-burning switches to the CNO cycle. Then, the local luminosity immediately increases and a new convective core appears (see Fig. 4). The onset of the CNO burning induces the typical expansion of the central regions (see Fig. 2) and also clearly marks the evolutionary tracks (see Fig. 3).

At the end of the H-burning the central temperature is so large ( $\sim 10^8$  K) that the He-burning immediately follows. These stars spend their central He-burning lifetime at the blue side of the HR diagram, thus omitting the first dredge up episode. For this reason, they enter the AGB phase with the original surface composition. As is usual at He ignition, a convective core develops, whose temporal evolution is shown in Figure 4. The H-burning shell, which forms immediately outside the H exhausted core, is particularly hot. The evolution of the temperature and that of the location (in mass coordinates) of the mesh where the energy generation rate of the H-burning is maximum, are shown in Figure 6 for the  $7 M_{\odot}$  model. Although the envelope is essentially lacking metals, the H-burning shell is mainly controlled by the CNO cycle. In fact, the temperature in the shell is large enough to allow for some carbon production via the  $3\alpha$  reactions. As a consequence, carbon is partially converted into nitrogen within the shell. The resulting internal profiles of hydrogen, carbon and nitrogen at the end of the central He-burning are illustrated in Figure 7.

#### 4. The early AGB phase

As is well known (see, for example, Becker & Iben 1979) during the early-AGB the H and the He burning are active in two separate shells. The energy generated by the He-shell induces an expansion and a cooling of the outermost layers, so that a convective envelope, which penetrates deeply within the star, develops. Though this is the first dredge up episode for these stars, we will call it second dredge up, due to the similarity with the one found in the more metal rich models.

The quantity (and the quality) of the matter dredged up to the surface differs significantly from that of more metal rich models and, as we will see below, this derives in the formation of two families of AGB stars. Let us note first that the amount of He dredged up by these P-IMS is much larger than that found in the more metal rich AGB stars. This is due to the fact that, since during most of the central hydrogen burning phase the main energy source is the PP-chain, He is produced in a wide region (in mass) of the stellar interior. The second important thing to note is that, since the  $3\alpha$  reactions are active up to the H-burning shell, primary carbon is dredged up. Some nitrogen also appears at the surface as a consequence of the mixing of material processed by the H-burning shell. Note that this is the only case in which the second dredge up alters the total abundance, by number, of the CNO group. In the lower panel of Figure 8 we show the variations, during the early-AGB, of the locations of the H and He-burning shells (as identified by the points where the nuclear energy production is maximum) as well as the extension of the convective envelope, for the  $7 M_{\odot}$  (no extra-mixing) model. The corresponding evolution of the surface abundances of C, N, O and He are shown in the upper panel. In Table 2 we have summarized some properties of our models at the end of the early-AGB, namely (in columns 1 to 7): the stellar mass, the assumed value of  $\beta$  (see the definition of this parameter in section 2), the mass of the He core and the surface mass fraction of  $^4\text{He}$ ,  $^{12}\text{C}$ ,  $^{14}\text{N}$  and  $^{16}\text{O}$ . Note that the amount of CNO nuclei in the envelope of these stars strongly depends on the initial mass.

Chieffi and Tornambé (1984) (see also Fujimoto et al. 1984) have shown that a minimum amount of CNO nuclei exists (roughly corresponding to a mass fraction of the order of  $10^{-7}$ ) for which the H-burning shell is fully sustained by the CNO cycle. This means that the stars in which the CNO abundance in the envelope is raised above this threshold value by the second dredge up will have a more or less standard H-burning shell, while the masses in which the amount of CNO catalysts remain below this threshold value are forced to raise the temperature in the H-burning region up to that typical of the He ignition. Also, in the latter case, the CNO cycle dominates the energy production in the H-burning shell, but its efficiency is

controlled by the amount of carbon locally produced via the  $3\alpha$  reactions. From the data reported in Table 2 it is evident that only for stellar masses larger than  $6 M_{\odot}$  is this minimum amount of CNO attained in the envelope at the end of the early-AGB. In fact, in these models the expansion and the cooling induced by the He-burning shell promptly allow a deep penetration by the convective envelope throughout the inter-shell region (see the lower panel of Fig. 8). For models having lower masses the inner edge of the convective envelope penetrates only slightly (or not at all) the H-He discontinuity and the resulting amount of CNO nuclei is definitely lower than the threshold value.

The results shown in the first 4 rows of Table 2 refer to models obtained using the Schwarzschild criterion to fix the boundaries of the regions mixed by convection. As discussed in section 2, we have also performed some tests to investigate the effects of a possible extra-mixing occurring below the border of the convective envelope. The results of these tests are given in the last 3 rows of Table 2. They indicate that such an extra-mixing has only a negligible effect on the efficiency of the second dredge up. A similar conclusion was previously obtained by Castellani, Marconi & Straniero (1998) for more metal-rich stars.

Before closing this section let us note that the  $8 M_{\odot}$  ( $Z=0$ ) model ignites carbon off-centre during the early-AGB. We followed part of this C-burning up to the formation of an extended convective shell and found that the minimum mass which is able to ignite carbon in a mildly degenerate core (usually called  $M_{up}$ ) is confined between the  $7 \leq M_{up}/M_{\odot} \leq 8$  for a generation of stars of zero initial metallicity, which confirms the previous result obtained by Tornambè & Chieffi (1986) and Cassisi & Castellani (1993).

## 5. The advanced AGB evolution

The early-AGB ends when the He shell, progressively approaching the H-He discontinuity, loses its efficiency and allows the overlying layers to contract and reheat. As a consequence, the H-burning shell reactivates and begins to accumulate fresh He on the underlying He core. This is the beginning of the so called thermally pulsing AGB phase (henceforth TP-AGB). When enough He is accumulated, the  $3\alpha$  reactions start again at the base of the He-rich layer. For the sake of completeness (for a more complete description of the TP-AGB stellar structures see the review of Iben & Renzini 1983) let us briefly note that in stars with *normal* metallicity the two shells (the H and the He ones) do not advance simultaneously in mass but, on the contrary, are active alternately. The He ignition is characterized by a rather strong thermonuclear runaway. The conditions of this He shell flash are somewhat different from those that lead to the He flash in a low mass star at the tip of the Red Giant Branch. The thermonuclear runaway, in the

latter case, is induced by the strong degeneracy of the electron component of the stellar plasma, while in TP-AGB stars the He-rich layer is largely non degenerate. If matter is non degenerate, the tendency for temperature to increase, due to the local release of thermonuclear energy, is normally counterbalanced by an expansion caused by the temperature dependence of the pressure. In most cases this pressure response rapidly quenches the heating and a quiescent (self-regulated) burning takes place. However, in TP-AGB models, the He ignition occurs in particular conditions (see Schwarzschild & Harm 1965) and the local temperature may rise for a certain time (how much mainly depends on the core mass) before the pressure response becomes effective. As the  $3\alpha$  reaction rate is strongly dependent on the temperature, the energy production rate of the He-burning shell rapidly increases up to  $10^6 - 10^8 L_\odot$ . The strength of the He flash depends, among other things, on the local values of temperature and density of the He-rich layer at the moment of the fuel ignition. For a given core mass, lower temperatures and larger densities imply higher He flash luminosities. It is important to note that these conditions are influenced by the rate at which the He-rich layer is accreted and, hence, by the properties of the H-burning shell. It is therefore clear that the amount of CNO catalysts in the envelope is a fundamental quantity that affects many properties of the TP-AGB phase, such as: the duration of the inter-pulse ( $\Delta t_{ip}$ ), the maximum  $3\alpha$  luminosity and the growth rate of the C-O core mass. For all these reasons one may expect a particular behaviour of the  $Z=0$  TP-AGB stars.

As already mentioned, Chieffi & Tornambé (1984) did not find thermal instabilities during the AGB of a  $5 M_\odot$  ( $Z=0$ ) stellar model. In fact they showed that, owing to the lack of CNO nuclei, the temperature in the H-burning shell is so high that the  $3\alpha$  reactions are active. Since the temperature at the base of the He-rich layer must be even higher, the two shells must be simultaneously active. In a companion paper Fujimoto et al. (1984) showed that under this condition, the stability of the He-burning shell depends on the core mass: those stars having a core mass larger than a critical value ( $\sim 0.73 M_\odot$ ) develop a stable He-burning shell, whereas for lower core masses thermal pulses occur. This prediction was confirmed by Chieffi & Tornambé: in their  $5 M_\odot$  model the two shells did advance (in mass) by consuming fuel at the same rate (at least within the phase that it was possible to compute at that time), so that a stable steady state was achieved during the AGB.

Concerning our set of P-IMS, let us discuss separately, for the sake of clarity, the more massive models, in which the second dredge-up is able to raise the CNO mass fraction in the envelope above the threshold value for a self-sustained CNO burning (i.e.  $\sim 10^{-7}$ ), and the less massive ones. It is important to note that all the present models develop a core mass, at the end of the early-AGB, larger than the critical value

obtained by Fujimoto et al. (1984).

### 5.1. $6 \leq M/M_{\odot} < M_{up}$

In these models the CNO cycle in the H-burning shell reaches its full efficiency at a temperature lower than the value needed to activate the  $3\alpha$  reactions. In this case the development of the thermally pulsing phase proceeds qualitatively as in the more metal rich AGB stars. The luminosity contributions of both the H and the He-burning shells, in the case of the  $7 M_{\odot}$  model and for two different values of the  $\beta$  parameter (see Section 2 and below), are shown in Figures 9 and 10. In Figures 11 and 12 we show the evolution of the corresponding locations (in mass coordinates) of the two shells as well as the extension of the convective envelope. Moreover some properties of these thermally pulsing models are listed in Tables 2 and 3, namely (in columns 1 to 8): the position of the H-burning shell at the onset of the thermal pulse (exactly when the He-burning luminosity becomes larger than the H-burning luminosity), the duration of the inter-pulse, the peak luminosity of the He-flash, the temperature of the H-burning shell (exactly at the point where the nuclear energy production is maximum) at He re-ignition, the density of the He-burning shell at He re-ignition and the surface mass fractions of  $^{12}\text{C}$ ,  $^{14}\text{N}$  and  $^{16}\text{O}$ . Firstly we note that, owing to the lower amount of CNO nuclei in the envelope, the temperature of the H-burning shell is higher than that typically found in more metal-rich models (see, for example, Straniero et al. 2000). For example, in a  $7 M_{\odot}$  model ( $Z=0.02$ ) we found, at the beginning of the  $10^{th}$  TP, that the temperature of the H-burning shell is  $\log T_H = 7.93$ , while in the present  $Z=0$ , even though the core mass is slightly lower, we find  $\log T_H = 8.10$ . As a consequence, the temperature of the He accumulated by the H-burning shell is higher and, in turn, a smaller density is required to start the  $3\alpha$  reactions. This occurrence becomes more evident if the properties of the He shell at the onset of a TP are compared to the corresponding ones in a model whose envelope has been enriched with fresh CNO catalyst. Figure 13 shows the evolution of the temperature, the density and the pressure of the He shell in the period between the  $9^{th}$  and the  $12^{th}$  TP of the  $7 M_{\odot}$  and  $\beta = 0.005$  model. In this period the surface CNO mass fraction is approximately constant ( $\sim 2.2 \cdot 10^{-6}$ ). The same quantities are given in Figure 14, but for the last computed TPs. In the latter case the mass fraction of CNO in the envelope grows from about  $6.4 \cdot 10^{-5}$  to  $1.33 \cdot 10^{-4}$ . Then, the larger the CNO abundance in the envelope the lower the temperature and the larger the density attained by the He-rich layer before the beginning of a TP. Note that in this case the duration of the inter-pulse is longer, because more time is needed to reach the conditions for the He ignition. The greater density of the He-rich material at the

moment of the re-ignition clearly implies a stronger thermal pulse. This is evident from Figures 9 and 10 (see also the third column in Tables 3 and 4).

In spite of the lower intensity of the thermonuclear runaway, in the present  $Z=0$  models, too, the He flashes induce the formation of a convective region which extends, after a few TPs, over the whole inter-shell region. In such a way, the products of the He-burning (essentially carbon) are distributed throughout the H-exhausted region. After each pulse, when the quiescent He-burning takes place at the base of the He-rich layer, the inner border of the convective envelope moves inward and closely approaches the H-He discontinuity. For example, at the 10<sup>th</sup> TP of the 7  $M_{\odot}$  models, the inner border of the convective envelope penetrates the H-burning shell reaching a layer which is only  $\sim 10^{-5} M_{\odot}$  away from the C-enhanced region. Note that this situation has also been found in the case of a mixing strictly confined within the boundary defined by the Schwarzschild criterion. Becker and Iben (1979) were first to note that this is a very promising case, in which an overshoot may be activated owing to the *”finite and positive value of  $\nabla_{rad} - \nabla_{ad}$  at the base of the formal convective zone”*. They found that this happens when the amount of He-rich material that remains below the convective envelope is less than about 0.1  $M_{\odot}$ . Such a condition is very soon fulfilled (after about 4 or 5 TPs) in our  $Z=0$  models that have a mass larger than 6  $M_{\odot}$ . The resulting *induced overshoot* may be of great relevance for the possible dredge up of carbon-rich material. This carbon dredge up, which is commonly named the third dredge up (henceforth TDU), has been invoked to explain the formation of the present generation of carbon stars (Iben 1975) and it is strongly supported by the observational evidence that there exists an evolutionary sequence of the various AGB components (from M to S and C stars) characterized by a progressive increase in the C/O ratio. As explained in Section 2 we have activated this induced overshoot by artificially adding a small extra-mixing below the base of the convective envelope. In order to check the dependence of the resulting dredge up from the assumed strength of the extra-mixing we have computed various models by changing the free parameter  $\beta$  in equation (5). In all the cases in which an extra-mixing below the formal convective envelope has been included, a deep carbon dredge up is obtained. Note the two different regimes that characterize the TP-AGB evolution before and after the first C-dredge up episode (see Figures 9 to 12 and Tables 3 and 4). For few TPs, the C-dredge up induces a rapid H re-ignition (this is evident in the upper panels of Figures 9 and 10). For  $\beta \geq 0.02$  the first H thermonuclear runaway is particularly strong (the peak luminosity is larger than  $5 \cdot 10^6 L_{\odot}$ ). To follow this phase our adaptive mesh algorithm puts more than 5000 mesh points in the convective envelope, 3000 just in the innermost 0.1  $M_{\odot}$ . In this case the mixing algorithm described in Section 2 consumes a huge amount of computer time (about 3 days to compute one dredge up episode on a 700 MHz

workstation). For this reason we have followed only two C-dredge up episodes in the  $\beta = 0.02$  case and just one in the  $\beta = 0.04$  case. Note that the total amount of CNO dredged up in the first episodes of C-ingestion in the  $\beta = 0.02$  case (about  $5 \cdot 10^{-4} M_{\odot}$ ) is equivalent to that cumulatively ingested during five dredge up episodes in the  $\beta = 0.005$  case. It is clear that, owing to the increase in the CNO in the envelope, the temperature of the H-burning shell and the strength of this H flash are progressively reduced (see column 4 of Tables 3 and 4 and Figures 9 and 10) until this peculiarity of the Z=0 TP-AGB models also disappears. Let us finally note that Herwig (2000) did not find a clear dependence of the dredge up efficiency on the extra-mixing efficiency. Perhaps this discrepancy may be due to the different chemical composition of the Herwig models (namely Z=0.02). Nevertheless his tests were made by changing the parameter that control the extra-mixing for just one TP. We suspect that a more evident variation of the dredge up should be found if the AGB evolution is followed for several TPs (as we actually do in the present paper) under different assumption for the extra-mixing efficiency. In any case, the great relevance of the dredge up on our capability of predict the AGB properties demands a deeper analysis of this question which is evidently beyond the scope of the present paper.

## 5.2. $4 \leq M/M_{\odot} < 6$

The scenario described above holds for the more massive P-IMS, for which the CNO abundance in the envelope is raised by the second dredge up above the threshold value which allows the full efficiency of the H-burning shell without the requirement of additional CNO catalysts coming from a local production of carbon. This condition implies the formation of fairly normal AGB stars. On the contrary, the behaviour of the less massive Z=0 stars is rather peculiar.

Figure 15 shows, for a  $4 M_{\odot}$  ( $\beta = 0.01$ ) model, the H and He luminosities as a function of the time, while Figure 16 shows the locations (in mass coordinates) of the He and the H-burning shells and the extension of the convective envelope as a function of time. Table 5 lists some properties of the same model.

The first thing worth noting is that, though the CNO mass fraction in the envelope is lower than  $10^{-7}$  and though the core mass is larger than the critical upper limit found by Fujimoto et al. (1984), these AGB models experience thermal instabilities. The H-burning is indeed regulated by the carbon locally produced via the  $3\alpha$  reactions, but the coupling of the H and the He-burning is so weak that they do not advance (in mass) at the same rate. As a consequence, small amplitude thermal pulses take place. Owing to the weakness of these He-shell flashes, the inner border of the convective envelope does not penetrate the

He-rich layer so that the induced overshoot is probably not activated.

The second, very important occurrence is that since the first thermal pulse the H shell becomes unstable and a convective zone develops (hereinafter HCE: Hydrogen Convective Episode), whose maximum extension is attained just after the usual He convective episode (HeCE) starts to shrink and just before the convective envelope reaches its maximum inward penetration. Let us stress that these new convective episodes are a systematic property of these  $Z=0$  AGB models with masses ranging between 4 and  $6 M_{\odot}$ . The base of this HCE closely approaches the border of the carbon-enriched zone left by the HeCE in the inter-shell. This condition is similar to the one already encountered when the convective envelope penetrates the H shell (see previous subsection). In fact, owing to the greater opacity of the H-rich material, a discontinuity of the radiative gradient forms at the interface between the base of the HCE and the He-rich layer below. This condition is favourable to the induced overshoot that, in our opinion, would easily extend the base of the HCE down to the C-enhanced layer. In such a case, the carbon ingestion would induce a sudden thermonuclear runaway of the H-burning shell.

The consequences of this mixing event are illustrated in Figures 16 and 17. In this particular case the two shells move simultaneously outward for some time, but, when the innermost burning front gets closer to the H-He discontinuity, its rate relaxes. From now on, weak thermal pulses take place, characterized by the two convective episodes described above: the standard HeCE and the unusual HCE. During the 5<sup>th</sup> TP the HCE extends inward and overlaps the region previously mixed by the He convective shell. This situation is illustrated in Figure 17. Then carbon is dredged up and immediately a H flash occurs. The energy released by this second (H) flash makes an important contribution to the expansion of the outermost layers started by the first (He) flash. Later on, during the post-flash period, the convective envelope penetrates the H-burning region. Thus, the surface abundances of C and N are significantly enhanced (the CNO mass fraction in the envelope becomes  $\sim 4 \cdot 10^{-6}$ ). This is an irreversible phenomenon since the amount of C dredged up is now so large that the star behaves, from now on, like the more massive ones. In particular after a few more TPs, the *standard* TDU takes place.

Note that in a model computed with a mixing strictly confined within the boundaries formally defined by the Schwarzschild criterion, the base of the HCE comes very close to the ex-convective shell generated by the thermal pulse and the occurrence of the carbon dredge up is arbitrarily dependent on the accuracy of the computation. Our experiments show that by changing the number of time steps and/or the spatial resolution, the HCE may or may not penetrate the C-rich region below it. However, once a small

extra-mixing is included (even just by putting  $\beta = 0.001$  in equation (5)) this uncertainty disappears and the carbon dredge up at the base of the HCE is systematically obtained after a few TPs. In the particular case illustrated in figures 15, 16 and 17 a first close approach of the HCE to the C-rich inter-shell region has been obtained after just 3 TPs (see column 6 of table 5), but only the fifth one is capable to dredge up enough C to turn off the AGB evolution of this model. In our opinion the case in which the HCE does not enter the carbon rich layers is unrealistic since it comes, in any case, so close to the C-rich region that any small instability would lead to the irreversible and definitive mixing that brings the AGB properties of these models towards those of the more massive ones.

## 6. Conclusions

The occurrence of thermal pulses in primordial AGB stars with masses ranging between 4 and 8  $M_{\odot}$  implies a major revision of the early nucleosynthesis scenario. We have shown that models with  $M \geq 6 M_{\odot}$  develop a deep convective envelope that penetrates the H shell and approaches the region previously enriched with the carbon produced during the He shell flash. Moreover we have demonstrated that in this condition even a small extra-mixing occurring below the base of the convective envelope induces a significant carbon dredge up. We note that the abundances measured in the present generation of AGB stars demand the occurrence of the third dredge up (see, for example, the review of Iben & Renzini 1983 and references therein). Then, the fresh carbon engulfed in the envelope is partially converted into nitrogen by the CNO burning occurring at the base of the convective region. Thus these AGB stars develop C and N rich envelopes.

Our models with masses ranging between 4 and 6  $M_{\odot}$  start the TP-AGB phase with weak He shell flashes so that the base of the convective envelope remains far from the H-burning shell. We show, however, that immediately after a thermal pulse, the H-burning shell becomes convectively unstable and the inner border of this convective region (HCE) closely approaches the C-enriched zone. Also, in this case, we believe an induced overshoot is likely to occur. In our models, which include a small additional mixing at the base of the HCE, a thermonuclear runaway is activated by the carbon ingested by the HCE. The resulting expansion of the outermost layers leads to the deep penetration of the convective envelope that overlaps the whole region previously mixed by the HCE. Then the abundance of CNO in the envelope rises enough to allow a *normal* AGB evolution from now on. In particular, after a few TPs, the TDU may further increase the carbon abundance in the envelope so that, once again, it is partially converted into nitrogen by the

CNO burning occurring at the base of the external convective region.

The precise evaluation of the amount of nitrogen and carbon produced by these primordial AGB stars depends on the value of the parameter used to describe the strength of the extra-mixing ( $\beta$  in our equation (5)). The uncertainty concerning the mass loss rate is a further (important) limit to our comprehension of the nucleosynthesis contribution from these stars. Any attempt to calibrate these free parameters encounters the problem of the scarcity of observable constraints for population III stars. Note, however, that though a quantitative derivation of the nucleosynthesis products requires a precise determination of the efficiency of mass loss and convective mixing, the new evolutionary scenario for P-IMS emerging from our models is not substantially affected by the above uncertainty.

The imprint of this nucleosynthesis could be sought in the more metal deficient stars presently observed in our Galaxy and in the high redshift Lyman  $\alpha$  systems. Observations show solar and relatively flat [C/Fe] and [N/Fe] ratios with metallicity which indicates a primary origin of both elements (see, for example, McWilliam 1997 and references therein). The nucleosynthesis of massive stars is sufficient to explain the primary carbon observed in metal poor halo dwarfs, but it cannot account for the primary nitrogen (Timmes, Woosley & Weaver 1995). In a companion paper (Abia et al. 2001) we investigate the implications of the new models for population III stars on the chemical evolution of the early galaxy. We show that the P-IMS models presented here, coupled with our new models for massive  $Z=0$  stars (Limongi, Straniero & Chieffi 2001) allow us to reproduce the primary behaviour of both C and N down to the lowest observed metallicity. For example, by using the P-IMS computed assuming  $\beta = 0.01$  we obtain  $-0.3 \leq [N/Fe] \leq +1.0$ , the precise value depending on the assumed initial mass function and on the iron amount ejected by  $Z=0$  SNII (see also Domínguez et al. 2000).

Recently, it has been pointed out that a considerable fraction (20-25%) of the most metal poor stars are carbon-rich,  $[C/Fe] \geq 1$  (Rossy, Beers & Sneden 1999). In most cases these extremely metal poor carbon stars are also nitrogen-enhanced (Norris, Ryan & Beers 1997; Bonifacio et al. 1998; Hill et al. 2000). Fujimoto, Ikeda & Iben (2000) suggest that some of these carbon stars may be the product of mass transfer from an AGB companion of mass lower than  $3 M_{\odot}$  in close binary systems. Our computations show that in the case of an intermediate mass companion, too, the surface composition of the secondary star after the mass transfer episode should be CN enhanced.

Another interesting product of the nucleosynthesis occurring in these P-IMS models is Li. When the temperature at the base of the convective envelope is higher than  $20 - 30 \cdot 10^6$  K, beryllium is efficiently

produced through the  ${}^3\text{He}({}^4\text{He},\gamma){}^7\text{Be}$  reaction. Then,  ${}^7\text{Li}$  is synthesized via the electron capture of  ${}^7\text{Be}$ , whose terrestrial half life is about 53 days. If this electron capture occurs at the base of the envelope, the resulting Li would be immediately destroyed as a consequence of the  ${}^7\text{Li}(\text{p},\alpha){}^4\text{He}$  reaction. However the convective motion might be so fast that most of the beryllium produced at the base of the envelope is redistributed in the outermost layers of the star, where the temperature is lower and Li is preserved. This is the well known Cameron-Fowler mechanism (Cameron 1955). In our models of P-IMS such a process is particularly efficient during the TP-AGB phase so that the mass fraction of Li in the envelope increases to a value comparable with the one expected from the big bang nucleosynthesis (see, for example, Walker et al. 1991).

Let us finally mention an interesting nucleosynthesis channel that may be activated in zero metal AGB stars by the production of free neutrons. As is well known (see, for example, Busso, Gallino & Wasserburg 1999), the main component of the cosmic s-elements has been synthesized by neutron captures on iron seeds occurring in TP-AGB stars. Being deprived of iron, P-IMS cannot contribute to this nucleosynthesis. However, if the two major neutron sources, namely the  ${}^{22}\text{Ne}(\alpha,\text{n}){}^{25}\text{Mg}$  and the  ${}^{13}\text{C}(\alpha,\text{n}){}^{16}\text{O}$  reactions, are activated they might contribute to the synthesis of lighter elements. We found that the  ${}^{14}\text{N}$  left by the advancing H-burning shell is fully converted into  ${}^{22}\text{Ne}$  during the TP. Obviously, as this nitrogen depends on the amount of CNO in the envelope, the amount of  ${}^{22}\text{Ne}$  in the convective region generated by the He flash is rather small at the beginning of the TP phase. However, after some dredge up episodes this value increases significantly. As an example, in the last computed TP of the  $4 M_{\odot}$  ( $\beta = 0.01$ ), the mass fraction of  ${}^{22}\text{Ne}$  in the inter-shell region is about  $5 \cdot 10^{-3}$ , which is about half the value typically found in AGB models of solar chemical composition. In our  $Z=0$  models the maximum temperature at the base of the convective zone generated by the He shell flash ranges between 310 and  $350 \cdot 10^6$  K so that the  ${}^{22}\text{Ne}(\alpha,\text{n}){}^{25}\text{Mg}$  is definitely involved. Since the amount of  ${}^{22}\text{Ne}$  in the inter-shell increases with time and since the temperature at the bottom of the convective shell also increases, the neutron production and the related nucleosynthesis would be particularly efficient in the final part of the TP-AGB phase of these P-IMS. For these reasons many more models are needed to calculate this neutron capture synthesis. Nevertheless the release of free neutrons (at least from the  ${}^{22}\text{Ne}$  source) in an environment lacking iron seeds should activate a particular nucleosynthesis channel whose product could be used to trace the pollution caused by the missing population III in the primordial galactic material.

This work has been partially supported by the MURST Italian grant Cofin2000, by the MEC Spanish

grant PB96-1428, by the Andalusian grant FQM-108 and it is part of the ITALY-SPAIN integrated action (MURST-MEC agreement) HI1998-0095. A. Chieffi thanks the Astronomical Observatory of Rome and its Director, Prof. Roberto Buonanno, for the generous hospitality at Monteporzio Catone. I. Domínguez thanks everybody from the *Osservatorio Astronomico di Collurania* (Teramo, Italy) for their hospitality.

## REFERENCES

- Abel, T., Anninos, P.A., Norman, M.L., Zhang, Y. 1998, ApJ, 508, 518
- Abel, T., Bryan, G.L., Norman, M.L. 2000, ApJ, in press
- Abia, C. et al 2001, in preparation
- Alexander, D.R., Fergusson, J.W., 1994, ApJ, 437, 879
- Beers, T.C., Preston, G.W., Shectman, A., 1992, AJ, 103, 1987
- Becker, S.A., Iben, I.J., 1979, ApJ, 232, 831
- Bessell, M.S., Norris, J., 1984, ApJ, 285, 622
- Blöcker, T., 1995, A&A, 297, 727
- Bond, J.R., 1981, ApJ, 248, 606
- Bonifacio, P., Molaro, P., Beers, T.C., Vladilo, G. 1998, A&A, 332, 672
- Bromm, V., Coppi, P.S., Larson R.B. 1999, ApJ, 527, L5
- Busso, M., Gallino, R., Wasserburg, G.J., 1999, ARA&A, 37, 239
- Cameron, A.G.W., 1955, ApJ, 121, 144
- Carbon, D.F., Barbuy, B., Kraft, R.P., Friel, E.D., Suntzeff, N.B., 1987, PASP, 99, 335
- Carlberg, R.G. 1981, MNRAS, 197, 1021
- Carney, B.W., Peterson, R.C., 1991, ApJ, 245, 238
- Cassisi, S., Castellani, V., 1993, ApJS, 88, 509
- Castellani, V., Giannone, P., Renzini, A., 1971a, Ap&SS, 10, 340
- Castellani, V., Giannone, P., Renzini, A., 1971b, Ap&SS, 10, 355
- Castellani, V., Chieffi, A., Tornambè, A., 1983, ApJ, 272, 249

- Castellani, V., Chieffi, A., Straniero, O., 1990, ApJ, 74, 463
- Castellani, V., Marconi, M, Straniero, O., 1998, A&A, 340, 160
- Chieffi, A., Tornambè, A., 1984, ApJ, 287, 745
- Chieffi, A., Limongi, M., Straniero, O., 1998, ApJ, 737, 762
- Cowie, L.L., Songaila, A., Kim, T.S., Hu, E. 1995, AJ, 109, 1522
- de Araújo, J.C.N., Opher, R. 1989, MNRAS, 239, 371
- Domínguez, I., Chieffi, A., Limongi, M., Straniero, O., 1999, ApJ, 534, 226
- Domínguez, I., Abia, C., Straniero, O., Chieffi, A., Limongi, M., 2000, in *Nuclei in the Cosmos VI*, Nuclear Physics A, in press (astro-ph/0010365)
- Ellison, S.L., Songaila, A., Schaye, J., Pettini, M. 2000, AJ, in publication
- Eryurt-Ezer, D., 1981, Ap&SS, 79, 265
- Ezer, D., 1961, ApJ, 133, 159
- Ezer, D., Cameron, A.G.W., 1971, Ap&SS, 14, 399
- Ezer, D., 1972, Ap&SS, 18, 226
- Frost, C., Lattanzio, J., 1996, ApJ, 473, 383
- Fujimoto, M.Y., Iben, I. Jr, Chieffi, A., Tornambè, A., 1984, ApJ, 287, 749
- Fujimoto, M.Y., Ikeda, Y., Iben, I. Jr, 2000, ApJ, 529, L25
- Groenewegen, M.A.T., de Jong, T., 1993, A&A, 267, 410
- Groenewegen, M.A.T., de Jong, T., 1994a, A&A, 282, 127
- Groenewegen, M.A.T., de Jong, T., 1994b, A&A, 283, 463
- Haiman, Z., Thoul, A.A., Loeb, A. 1996, ApJ, 464, 523

- Herwig, F., 1995, in *Stellar Evolution: What should be done ?*, 32 Liege Int. Astr. Colloq., ed. A. Noels, D. Fraipon-Caro, M. Gabriel, N. Grevesse & P. Demarque (Liege: Univ. Liege), 441
- Herwig, F., Blöcker, T., Schönberner, D., El Eid, M., 1997, A&A, 324, L81
- Herwig, F., A&A, 2000, 360, 952
- Hill, V., Barbuy, B., Spite, M., Spite, F., Cayrel, R., Plez, B., Beers, T.C., Nordström, B., Nissen, P.E. 2000, A&A, 557
- Hollowell, D., Iben, I.J., 1989, ApJ, 340, 966
- Hollowell, D., Iben, I.J., Fujimoto, M.Y., 1990, ApJ, 351, 245
- Iben, I.J., 1975, ApJ, 196, 525
- Iben, I.J., 1981, ApJ, 246, 278
- Iben, I.J., 1982, ApJ, 260,821
- Iben, I.J., Renzini, A., 1982, ApJ, 259, L79
- Iben, I.J., Renzini, A., 1983, ARA&A, 21, 271
- Iglesis, C.A., Rogers, F.J., Wilson, B.G., 1992, ApJ, 397, 717
- Laird, J.B. 1985, ApJ, 289, 556L
- Lambert, D.L., 1991, in *Evolution of stars: the photometric abundance connection*, Eds. G. Michaud & A. Tutukov (Dortrecht:Kluwer), 299
- Langer, N., Heger, A., Wellstein, S., Herwig, F., 1999, A&A, 346, L37
- Larson, R.B. 1998, MNRAS, 301, 569
- Lattanzio, J.C. 1989, ApJ, 399, L25
- Lepp, S., Shull, M. 1983 ApJ, 270, 578
- Limongi, M., Straniero, O., Chieffi, A. 2000, ApJS, 129,625

- Limongi, M., Straniero, O., Chieffi, A. 2001, in preparation; *see*  
<http://www.mporzio.astro.it/mandrake/orfeo.html>
- McWilliam, A. 1997, *ARA&A*, 35, 503
- Molaro, P., Castelli, F., 1990, *A&A*, 228, 426
- Molaro, P., Bonifacio, P., 1990, *A&A*, 236, L5
- Mowlavi, N., 1999, *A&A*, 344, 617
- Nakamura, F., Umemura, M., 1999, *ApJ*, 515, 239
- Nakamura, F., Umemura, M., 2000, *ApJ*, submitted
- Norris, J.E., Ryan, S.G., Beers, T.C., 1997, *ApJ*, 489, L172
- Omukai, K., Nishi, R., Uehara, H., Susa, H. 1998, *Prog. Theor. Phys.*, 99, 747
- Paczyński, B., 1970, *Acta Astron.*, 20, 195
- Palla, F., Salpeter, E.E., Stahler S.W. 1983, *ApJ*, 271, 632
- Pettini, M., Smith, L.J., King D.L., Hunstead, R.W. 1997, *ApJ*, 486, 665
- Primas, F., Molaro, P., Castelli, F., 1994, *A&A*, 290, 885
- Rossi, S., Beers, T.C., Sneden, C., 1999, *Carbon Abundances for Metal-Poor Stars Based on Medium-Resolution Spectra in Third Stromlo Symposium: The Galactic Halo*, eds. Gibson and M. Putman (ASP: San Francisco), 165, 268
- Ryan, S.G., Norris, J.E., Bessels, M.C., 1991, *AJ*, 102, 303
- Ryan, S.G., Norris, J.E., Beers, T.C., 1996, *ApJ*, 471, 254
- Ryan, S.G., Norris, J.E., Beers, T.C., 1999, *ApJ*, 523, 654
- Schwarzschild, M., Härm, R., 1967, *ApJ*, 150, 961
- Shapiro, P.R., Kang, H. 1987, *ApJ*, 318, 32

- Silk, J., 1983, MNRAS, 205, 705
- Snedden, C., Preston, W.G., McWilliam, A. Searle, L., 1994, ApJ, 431, L27
- Songaila, A., Cowie, L.L. 1996, AJ, 112, 335
- Sparks, W.M., Endal, A.S., 1980, ApJ, 237, 130
- Straniero, O., Chieffi, A., Limongi, M., 1997, ApJ, 490, 425
- Straniero, O., Chieffi, A., Limongi, M., Gallino, R., Busso, M., Arlandini, C., 1997, ApJ, 478, 332
- Straniero, O., Chieffi, A., Limongi, M., Gallino, R., Busso, M., Domínguez, I., 2000, in *The Changes in Abundances in Asymptotic Giant Branch Stars*, eds. F. D’Antona and R. Gallino, MSAIt, in press.
- Timmes, F.X., Woosley, S.E., Weaver, T.A., 1995, ApJS, 98, 617
- Tytler, D., Fan, X.M., Burles, S., Cottrell, L., Davis, C., Kirkman, D., Zuo, L. 1995, in *QSO absorption lines*, ed. G. Meylan (Garching, ESO) 289
- Tornambè, A., Chieffi, A. 1986, MNRAS, 220, 529
- Uehara, H., Susa, H., Nishi, R. 1996, ApJ, 473, L95
- Walker, T.P., Steigman, G., Kang, H. S., Schramm, D.M., Olive, K.A. 1991, ApJ, 376, 51
- Wasserburg, G.J., Qian, Y.-Z. 2000a, ApJ, 529, L21
- Wasserburg, G.J., Qian, Y.-Z. 2000b, ApJ, 538, L99
- Weidemann, V., 1987, A&A, 188, 74
- Weidemann, V., 2000, A&A, 363, 647
- Yoshii, Y., Saio, H., 1986, ApJ, 301, 587

### FIGURE CAPTIONS

Fig. 1.— Isotopes included in the nuclear network; those identified by triangles have only been included during the H-burning.

Fig. 2.— Evolution of the central temperature as a function of the central density for the computed models.

Fig. 3.— Evolutionary tracks in the HR diagram of the computed models.

Fig. 4.— Evolution with time of the central convective regions up to the end of the He burning for the computed models: H-burning via the PP-chains (first episode), H-burning via CNO cycle (second episode) and He-burning (third episode).

Fig. 5.— Evolution with time of the central C abundance (mass fraction) for the computed models.

Fig. 6.— Evolution with time of the H-burning shell during the central He-burning phase for the  $7 M_{\odot}$  model. Lower panel: the position (in mass) where the nuclear energy generated by the H-burning shell is maximum. Upper panel: the temperature at the same point.

Fig. 7.— C (solid line), N (dashed line) and H (dotted line) mass fraction profiles of the  $7 M_{\odot}$  model at the end of the central He burning.

Fig. 8.— The early-AGB phase of the  $7 M_{\odot}$  model (no extra-mixing). Upper panel: evolution with time of the surface abundance (mass fraction) of C (long-dashed line), N (short-dashed line), O (dotted line) and He (solid line). Note that the He scale reads on the right Y axis. Lower panel: evolution with time of the location (in mass coordinates) of the H and He-burning shells. The dashed area shows the extension of the convective envelope.

Fig. 9.— Evolution with time of the H and He-burning luminosities during the TP-AGB phase in the case of the  $7 M_{\odot}$  ( $\beta = 0.005$ ) model. The initial time corresponds to the deepest penetration of the convective envelope after the  $2^{nd}$  dredge up.

Fig. 10.— Evolution with time of the H and He-burning luminosities during the TP-AGB phase in the case of the  $7 M_{\odot}$  ( $\beta = 0.01$ ) model. The initial time corresponds to the deepest penetration of the convective envelope after the  $2^{nd}$  dredge up.

Fig. 11.— Evolution with time of the location (in mass coordinates) of the H and the He-burning shells of the same models as in Figure 9. The dashed area shows the extension of the convective envelope.

Fig. 12.— Evolution with time of the location (in mass coordinates) of the H and the He-burning shells of the same models as in Figure 10. The dashed area shows the extension of the convective envelope.

Fig. 13.— Properties of the He-burning shell between the 9<sup>th</sup> and the 12<sup>th</sup> TP of the 7  $M_{\odot}$  ( $\beta = 0.005$ ) model: density (upper panel), temperature (central panel) and pressure (lower panel). The initial time corresponds to the deepest penetration of the convective envelope after the 2<sup>nd</sup> dredge up.

Fig. 14.— Properties of the He-burning shell between the 17<sup>th</sup> and the 20<sup>th</sup> TP of the 7  $M_{\odot}$  ( $\beta = 0.005$ ) model: density (upper panel), temperature (central panel) and pressure (lower panel). The initial time corresponds to the deepest penetration of the convective envelope after the 2<sup>nd</sup> dredge up.

Fig. 15.— Evolution with time of the H and He-burning luminosities during the TP-AGB phase in the case of the 4  $M_{\odot}$  ( $\beta = 0.01$ ) model. The initial time corresponds to the deepest penetration of the convective envelope after the 2<sup>nd</sup> dredge up.

Fig. 16.— Evolution with time of the locations (in mass coordinates) of the H and the He-burning shells of the same models as in Figure 15. The dashed area shows the extension of the convective envelope.

Fig. 17.— Evolution with time of the convective episodes (dashed regions) during (and immediately after) the 4<sup>th</sup> and 5<sup>th</sup> TP of the same models as in Figure 15. The two (approximately) horizontal lines represent the location of the H and He-burning shells. A first convective episode (HeCE) develops in the inter-shell region as a consequence of the TP. A second one starts later at the base of the H-rich envelope (HCE). During the 5<sup>th</sup> TP the innermost part of the HCE overlaps the region previously mixed by the HeCE; this induces two H flashes that produce the two evident tongues of the outer border of the HCE. Later on, the convective envelope moves inward and a dredge up of C and N occurs.